TOHOKU UNIVERSITY

Advanced Institute for Materials Research

Tohoku University

Annual Review 2011

東北大学原子分子材料科学高等研究機構

wpi World Premier International Research Center Initiative

AIMR Annual Review
Contents

2011 WPI-AIMR Main Events

Feb 21	WPI-AIMR is presented in Physics Today.
Mar 10	Dr. Khademhosseini was awarded "Sloan Research Fellowship"
Mar 10	Prof. M. Kawasaki (PI) will be awarded "8th Honda Frontier Award" for 2011.
April 14	Prof. Kurihara honored with "A. E. Alexander Lecture Award".
May 9	Prof. Takahashi (PI) was presented in Physics Today.
May 11	The paper by Assistant Prof. Sugawara was presented in AIP Advances. Assistant Prof. Sugawara's paper
May 11	Prof. Motoko Kotani was assigned as Deputy Director of WPI-AIMR.
June 3	WPI Program director, Dr. Kuroki's report on "WPI centers on March 11, 2011 and aftermath"
June 13	The paper by Dr. Khademhosseini's group is listed as the top downloaded paper.
July 8	The paper by Prof. Takahashi's group is selected for one of the most cited articles.
July 19	Prof. Itaya (PI) honored with "The Prix Jacques Tacussel Award of the International Society of Electrochemistry".
Aug 22	Prof. (PI) Adschiri's review "Green Materials With Supercritical Water" was selected for the top ten accessed articles.
Aug 29	Recruitment Program of Global experts by Chinese Government
Sep 12	Research Asso. Kubota's paper has been selected as Research Highlights in Journal of Applied Physics
Oct 3	Dr. Khademhosseini, Junior PI, was awarded "Presidential Early Career Award for Scientists and Engineers (PECASE)*" from the White House.
Oct 17	Dr. Khademhosseini, Junior PI, was awarded "Pioneers of Miniaturization Prize 2011" by the Royal Society of Chemistry's Lab on a Chip Journal.
Nov 2	The paper by Research Associate Xianmin Zhang (Miyazaki Group) has been selected for the October 31, 2011 issue of Virtual Journal of Nanoscale Science &
Nov 7	Vietnam's Prime Minister Dung visited WPI-AIMR.
Nov 10	AIMR signed MOU on academic exchange with Fraunhofer Institute for Electronic Nano Systems.
Nov 14	Research result from Takahashi group on a topological insulator was published in Nature Physics, and the experimental data measured by his group were selected as the cover design.
Nov 18	Prof. Ikuhara (PI) was awarded "Fellow, The American Ceramic Society".
Nov 21	Dr. Khademhosseini, Junior PI, selected as the 2012 Biotechnology and Bioengineering Daniel I.C. Wang Award recipient.
Dec 13	Completion Ceremony of the WPI-AIMR Main Building
Dec 13	The paper by Dr. Hongwen Liu "Single molecule detection from a large-scale SERS-active Au79Ag21 substrate" was selected as highlight in Nature Asia.

See the followin URL for more details: http://www.wpi-aimr.tohoku.ac.jp/en/modules/newsinfo/

Award Information

Name	Position	Thrust	Name of Award	Awarding Organization	Date of Award
Zhongchang Wang*	Assistant Prof.	Materials Physics	Award for Encouragement of Research of Materials Science	The Materials Research Society of Japan	Jan
Daisuke Ishii*	Assistant Prof.	Device/System	Award for Encouragement of Research of Materials Science	The Materials Research Society of Japan	Jan
Kazue Kurihara	PI	Soft Materials	A. E. Alexander Lecture	Royal Australian Chemical Institute	Jan
Ali Khademhosseini	Junior PI	Device/System	Sloan Research fellowship	Alfred P. Sloan Foundation	Feb
Yuichi Ikuhara	PI	Materials Physics	Humboldt Research Award	Alexander von Humboldt Foundation	Mar
Daisuke Ishii*	Assistant Prof.	Device/System	SSSJ Young-Researcher Lecture Award 2010	The Surface Science Society of Japan	February
Kazunori Ueno	Assistant Prof.	Materials Physics	Tokin Foundation for Advancement of Science and Technology 22th Research	NEC Tokin Corporation	March
Tomokazu Matsue	PI	Device/System	The Chemical Society of Japan Award for Creative Work	The Chemical Society of Japan	March
Tomokazu Matsue	PI	Device/System	Best Paper Award	The Electrochemical Society of Japan	March
Ali Khademhosseini	Junior PI	Device/System	Young Investigator Award	Society for Biomaterials	April
Mingwei Chen	PI	BMG	The 2011 Distinguished Award	The 8th International Workshop on Intermetallic and Advanced Materials, China	May
Esashi Group		Device/System	Outstanding Paper Award	Transducers	June
Ali Khademhosseini	Junior PI	Device/System	2011 Y.C. Fung Young Investigator Award	American Society for Mechanical Engineers (ASME)	June
Alain Reza Yavari	PI	BMG	Award for Scientific Excellence	French National Center for Scientific Research (CNRS)	July
Ali Khademhosseini	Junior PI	Device/System	Early Career Award in Nanotechnology	IEEE Advancing Technology for Humanity	August

Award Information

Name	Position	Thrust	Name of Award	Awarding Organization	Date of Award
Shinya Nakano	Research Assistant	Soft Materials	Poster Award of The 63th Divisional Meeting on Colloid and Interface	Divisional Meeting on Colloid and Interface Chemistry (DMCIC)	September
Ali Khademhosseini	Junior PI	Device/System	Pioneers of Miniaturization Prize 2011	The Royal Society of Chemistry's "Lab on a Chip Journal"	October
Ali Khademhosseini	Junior PI	Device/System	Presidential Early Career Award for Scientists and Engineers (PECASE)	The White House, the USA	October
Yuichi Ikuhara	PI	Materials Physics	Fellow, the American Ceramics Society	The American Ceramics Society	October
Ali Khademhosseini	Junior PI	Device/System	The 2012 Biotechnology and Bioengineering Daniel I.C. Wang	Biotechnology & Bioengineering Journal	November
Shinya Nakano	Research Assistant	Soft Materials	Poster Prize Runner-Up	12th Australia-Japan Colloid & Interface Science Symposium	November

FY2011 List of Major Governmental Research Funds
(As of August 1, 2011)

A. Grant-in-Aid for Scientific Research (KAKENHI)

(Unit: thousand yen)

Categories	Representative's Name		Budget Distribution (*1)
Scientific Research on Priority Areas	TANIGAKI, Katsumi (PI)		15,100
	TANIGAKI, Katsumi (PI)		13,300
	ASAO, Naoki		2,100
	HITOSUGI, Taro		800
	Subtotal	4	31,300
Scientific Research on Innovative Areas	KURIHARA, Kazue (PI)		14,690
	ASAO, Naoki		3,510
	HAMADA, Ikutaro		1,950
	Subtotal	3	20,150
Scientific Research (S)	ESASHI, Masayoshi (PI)		4,810
	ADSCHIRI, Tadafumi (PI)		33,280
	YAMAGUCHI, Masahiko (PI)		36,400
	TAKAHASHI, Takashi (PI)		72,410
	Subtotal	4	146,900
Scientific Research (A)	KOTANI, Motoko (PI)		9,620
	TSUKADA, Masaru (PI)		9,880
	MIYAZAKI, Terunobu (PI)		6,240
	YAMADA, Kazuyoshi (PI)		11,570
	MATSUE, Tomokazu (PI)		13,910
	IKUHARA, Yuichi (PI)		14,820
	YAMAMOTO, Yoshinori (PI)		15,860
	Subtotal	7	81,900
Scientific Research (B)	NISHI, Toshio (PI)		650
	Subtotal	1	650
Scientific Research (C)	ASAO, Naoki		1,170
	TAKEUCHI, Akira		1,430
	SHIMOMURA, Masatsugu (PI)		910
	NAKAJIMA, Ken		2,210
	SAITO, Mitsuhiro		2,990
	Subtotal	5	8,710
Challenging Exploratory Research	KOTANI, Motoko (PI)		1,300
	ISHII, Daisuke		2,080
	NAKAYAMA, Koji		2,730
	ADSCHIRI, Tadafumi (PI)		2,080
	Subtotal	4	8,190
Young Scientists (A)	ISHII, Daisuke		3,510
	HITOSUGI, Taro		17,940
	HOJO, Daisuke		22,880
	Subtotal	3	44,330
Young Scientists (B)	LIU, Hongwen		650
	YOSHIDA, Shinya		1,560
	MCKENNA, Keith Patrick		1,040
	XU, Limei		1,170
	JIN, Tienan		2,340
	FUJINAMI, So		650
	OHSAWA, Takeo		650
	HIRATA, Akihiko		1,300
	WANG, Zhongchang		1,560
	LIU, Yanhui		1,560
	TANABE, Yoichi		3,510
	JI, Sungdae		1,430
	TSUKIMOTO, Susumu		2,470
	Subtotal	13	19,890
Subtotal		44	362,020

B. Other Grant-in-Aid

(Unit: thousand yen)

Representative's Name	Distributing Organization	Project Title	Budget Distribution (*1)
ESASHI, Masayoshi (PI)	Japan Society for the Promotion of Science (JSPS)	Funding Program for World-Leading Innovative R&D on Science and Technology	679,000
Subtotal		1	679,000

C. Research funds consigned from government directly

(Unit: thousand yen)

Representative's Name	Distributing Organization	Project Title	Budget Distribution (*1)
ADSCHIRI, Tadafumi (PI)	Japan Science and Technology Agency (JST)	Core Research Evolutional Science and Technology (CREST)	14,950
TSUKADA, Masaru (PI)	Japan Science and Technology Agency (JST)	Core Research Evolutional Science and Technology (CREST)	7,800
KURIHARA, Kazue (PI)	Japan Science and Technology Agency (JST)	Core Research Evolutional Science and Technology (CREST)	71,760
SHIMOMURA, Masatsugu (PI)	Japan Science and Technology Agency (JST)	Core Research Evolutional Science and Technology (CREST)	19,500
KOTANI, Motoko (PI)	Japan Science and Technology Agency (JST)	Core Research Evolutional Science and Technology (CREST)	37,713
YAMADA, Kazuyoshi (PI)	Ministry of Education, Culture, Sports, Science and Technology (MEXT)	Elementary Strategic Project	9,555
ESASHI, Masayoshi (PI)	Japan Science and Technology Agency (JST)	Strategic International Cooperative Program	4,620
ADSCHIRI, Tadafumi (PI)	New Energy and Industrial Technology Development Organization (NEDO)	Technical Development of Ultra-hybrid Materials (Technological Development of Contradictory Functional Materials by nano-scale Structure Control)	197,157
HITOSUGI, Taro	Japan Science and Technology Agency (JST)	Precusory Research for Embryonic Science and Technology (PRESTO)	22,880
NAKAYAMA, Koji	Japan Science and Technology Agency (JST)	Research Seeds Quest Program	5,200
FUJITA, Takeshi	Japan Science and Technology Agency (JST)	Research Seeds Quest Program	5,850
IWAYA, Katsuya	Japan Science and Technology Agency (JST)	Research Seeds Quest Program	5,200
SATO, Toyoto	Japan Science and Technology Agency (JST)	Research Seeds Quest Program	2,950
HITOSUGI, Taro	New Energy and Industrial Technology Development Organization (NEDO)	Grant for Industrial Technology Research (Financial support to young researchers)	9,750
Subtotal		14	414,885

D. Research funds reconsigned through the private enterprise/university

(Unit: thousand yen)

Representative's Name	Distributing Organization	Redistributing Organization	Budget Distribution (*1)
NISHI, Toshio (PI)	New Energy and Industrial Technology Development Organization (NEDO)	Bridgestone Corporation	13,908
SHIMOMURA, Masatsugu (PI)	New Energy and Industrial Technology Development Organization (NEDO)	Fujifilm Corporation, Japan Tissue Engineering Co., Ltd. (J-TEC)	9,300
TSUKADA, Masaru (PI)	Japan Science and Technology Agency (JST)	Advanced Algorithm and Systems Co., Ltd.	3,120
TSUKADA, Masaru (PI)	Ministry of Education, Culture, Sports, Science and Technology (MEXT)	University of Tokyo	7,000
TANIGAKI, Katsumi (PI)	Misitry of Economy, Trade and Industry (METI)	Kuramoto Co., Ltd.	2,394
HITOSUGI, Taro	Japan Society for the Promotion of Science (JSPS)	University of Tokyo	30,193
Subtotal		6	65,915

Total	65	1,521,820

*1:Budget includes indirect expenses.

The Fourth Series of WPI-AIMR Joint Seminars FY2011

The topics of the Fourth WPI-AIMR Seminar Series of Fiscal Year 2011 are "Cooperation between Materials Science and Mathematical Science" and composed of two parts, i.e., (1) "Mathematical (Math-Mate) lecture + discussions", and (2) "Materials science presentation + discussion" meetings. The first half of the seminar is assigned to lecture/presentation, and the latter half to questions/ (panel) discussions. Initial several Seminars should be introductory to form a common understanding among WPI staffs on the aim/problems of the collaboration with mathematics.

As for the part (2), the speakers are chosen from younger/senior researchers mainly from WPI-AIMR and they provide topics concerning on the following questions;

[1] How does he/she expect the cooperation with mathematics or mathematical science?

[2] What does he/she expect from the concept of "Functon（see below）"
for creating a novel research strategy of materials science?

[3] How can his/her research topics be seen from the view point of Functon?

Proposals of a presentation at the Seminar providing any opinions and related topics by research members at WPI-AIMR will be most welcome. But Committee members of Seminars may ask research members to give a talk at one of the Seminars at any occasion.

Please remind that the participation to this Seminar Series is mandatory.

＊＊＊ about Functon ＊＊＊

Definition of the concept of "Functon" itself is the important theme which will be discussed through this seminar series. Here is a starting point for you to think of it by yourself.

What is Functon（"機能子" in Japanese and Chinese）?

Functon is a constituent element of materials showing a certain definite function or property, and every material is composed of one or many kinds of assembled functons. The size of functons ranges over from the size of atom/molecule to macroscopic size. Functons often take spatial or temporal nesting structures, i.e., the structures like matryoshka (Russian doll); higher rank functon is formed as an assembly of lower rank functons.

Why Functon?

Functon is a central concept introduced at WPI-AIMR to create a novel research strategy of materials science. Namely we consider materials science can be performed without going back to atom/molecule, but by introducing the concept of minimum function unit, i.e., functons. Working on functons, materials science can be effectively executed with a help of mathematical science. So far existing materials science remained the science of matter where properties of matter is solved in turn from the lower to higher rank, i.e., from atom/molecule level to macroscopic level, which therefore treats ordinary (non-inverse) problems in terms of mathematics. However, a true materials science should treat an inverse problem to finding out necessary functons to create novel materials with desired function. Mathematical science should play important role for that cooperating with materials science.

Functons as a target of mathematical sciences

Mathematical science, of which important tool is the concept of functon helping a bridge with the materials science, is needed for solving the difficult inverse problem. It should solve how to combine complicated multilayer functon systems for the inverse problem. Furthermore the mathematical science is also expected to help developing materials as sensitive but robust, and those with multi-functions responding environment change. Mathematics is also necessary for the control of rare events, and for device processes utilizing pattern formation and so on. These can be also achieved with the help of the concept of functons.

Establishing the concept of Functon

Elucidation of easy processes forming higher rank functons from the lower rank functons, even from those of atoms/molecules level, and forming functons in artificial materials, which are related with non-equilibrium open systems, phase transition and nucleation core, interface processes, and self-organization, have been major topics of individual materials science so far. However, to create a guiding principle of innovative materials science, it is essentially important to explore and establish a general concept of “Functon”, and with its bolster, establishing a strategy of a novel materials design by solving the inverse problem.

Report on the 1st Seminar

Nobuaki Aoki

June 24, 2011

"A Role of Mathematics in a New Context
– Seek for Possible Collaborations with Materials Science"
Prof. Motoko Kotani

"Algorithms for Segment Packing and Generalized Kakeya's Problem"
Prof. Takeshi Tokuyama (GSIS, Tohoku University)

Panel Discussion

The main topic of the 4th WPI-AIMR Joint Seminar Series is "Cooperation between Materials Science and Mathematical Science", and having the knowledge on the relationship between mathematics and materials science is the first step for establishing the cooperation. In the 1st seminar, we had two mathematical lectures and held panel discussion as a starting point of our scientific exploration.

For the first math lecture, Prof. Kotani presented change in the historical role of mathematics. She pointed out problems the human society encounter have become more and more complicated and larger in data-size in the late 1980s, and complexity beyond the efficiency zone of the existing tools encourages mathematics to acknowledge a new position to handle them. Earlier applications by European Science Foundation were also introduced and examples of successful collaboration with materials science were reported.

In the second lecture, Prof. Tokuyama illustrated a suggestive instance of solving a problem with the help of accumulation of mathematics over the past hundred years. The problem was to determine the smallest area from given line segments. It was solved in the context of computer science, but finding optimal geometric structures should be an important theme also in material science. He mentioned that such a solving methodology may bridge mathematics and computational material science.

The panel discussion was also held. In order to promote the cooperation with mathematics, we started comprehensive consideration on the materials science as the combination of element of functions. Following the introductory talk by Dr. Akagi, several examples of "functional unit (electric circuit, structure of document, concentration blob in polymer, *etc.*)" were given by the organizing committee, which include a suggestive clue to find a non-material functional unit in materials science.

Report on the 2nd Seminar

Ryo Nouchi

July 8, 2011

""Functon" in Adschiri Group's Research, Fusion of Ideas in WPI, Analogy & Math"
Prof. Tadafumi Adschiri

"What Is Functon, Why Functon and What Can Be Functon"
Prof. Katsumi Tanigaki

Panel Discussion

In this seminar, two Math-Mate talks were given by Prof. Adschiri and Prof. Tanigaki, which were followed by open discussions entitled "What can be *Functon* (2)" and "*Functon* as a Bridge between Materials Science and Mathematics". In succession to the 1st seminar, the efforts were made to help materials scientists think of the possible collaboration with mathematics.

In the first lecture, Prof. Adschiri emphasized needs for high heat conductive materials to make an efficient recovery system of exhaust heat from automobiles. To obtain materials possessing this function, Adschiri group has developed super hybrid materials such as surface-modified nanoparticles, which can be a basic functional element of this function. He also introduced the research results in WPI-AIMR, which unveiled similarities between different materials. This kind of analogy between different materials can be found further in other materials with the help of mathematics.

In the second lecture, Prof. Tanigaki mentioned three inventions that have most contributed to science and technology: namely, lasers, transistors, and integrated circuits. Next, he introduced main research subjects in Tanigaki group, *i.e.*, light-emitting organic transistors, Dirac-cone states in Fe-based superconductors, and cage-like thermoelectric materials. He also discussed possible basic functional elements for these three subjects. Finally, he encouraged us to make researches for energy harvesting without using pseudoscience like Feynman's ratchet.

Following the two Math-Mate talks, we had open discussions, which were led by Dr. Akagi. At first, Dr. Ikeda made an introductory talk about the role/importance of mathematics to establish a new scientific principle in materials science. After that, in succession to the previous seminar, we discussed about re-examination of functional materials as a combination of basic functional elements in order to make effective collaborations with mathematics.

Report on the 3rd Seminar

Taro Hitosugi and Kazuto Akagi

July 29, 2011

Topological Crystallography
– Commemorating the fourth centennial anniversary of the publication of Kepler's pamphlet “New-Year's gift concerning six-cornered snow” (1611) –
Prof. Toshikazu Sunada (Meiji University)

One-dimensional exotic-nanocarbon: Electrons in a Riemannian space
Prof. Jun Onoe (Tokyo Institute of Technology)

In this seminar, two talks were given by Profs. Sunada and Onoe, both encouraging our efforts to help materials scientists think of the possible collaboration with mathematics.

In the first lecture, mathematician Prof. Sunada gave a brief history of crystallography, a practical science that originated in the classification of the observed shapes of crystals, to provide the audience with a mathematical insight into modern crystallography. Then the talk went in to the formulation of a minimum principle for crystals in the framework of discrete geometric analysis, and predicted a new crystal based on K4 structure.

He expects the synthesis of the predicted material, and emphasized that topological crystallography vigorously interacts with other fields in pure mathematics and also with materials science.

The next speaker, a materials scientist Prof. Onoe, talked about their observation of Riemannian geometrical effects on the electronic properties of materials such as Tomononaga-Luttinger liquids, which were previously theoretically predicted by their group. They have examined a one-dimensional metallic C_{60} polymer with an uneven periodic peanut-shaped structure using *in situ* high-resolution ultraviolet photoemission spectroscopy.

Their successful combination of materials science and mathematics was quite impressive, and suggests one of the ways of research in WPI-AIMR.

Report on the 4th Seminar

Kazuto Akagi

August 26, 2011

"A map of mathematics for materials scientists"
Kazuto Akagi

"Why mathematics?"
Prof. Masatsugu Shimomura

In the past three seminars, we had several Math-Mate talks and open discussions on what we are aiming for through the fusion with mathematics. This attempt looks basically going well so far, but it is also true that we cannot well imagine "what really becomes possible by collaboration with mathematicians", still now. Therefore, two talks introducing how to interact with mathematics were given at this timing.

In the former part of the talk by Akagi, the world of mathematics was overviewed with simplified explanations on each field. Next, an example was introduced how chaos theory helped to analyze and stabilize the behavior of a furnace based on very limited numbers of monitoring data and a simplified physical model. Materials scientists are more or less familiar with the basic scientific framework (e.g. classical mechanics, thermodynamics, electromagnetics, statistical mechanics, quantum mechanics) and use it in their thinking. In the same way, we need to know minimum level of knowledge about the framework of mathematics (= a map of mathematical world) though we need not do mathematics itself, he said.

In the second talk, Prof. Shimomura gave a talk on "why mathematics" based on his experiences of collaboration with mathematicians in the field of biomimetics. One of the impressive examples was the biomimetics database aiming for contribution to other wide scientific and engineering fields including materials science. It is based on the digital image processing technology developed by Prof. Haseyama (Hokkaido Univ.), which helps us recognize buried similarity or relevance in enormous data one after another. As Prof. Nishiura says, mathematics is a ubiquitous tool.

Report on the 5th Seminar

Kazuto Akagi

October 6, 2011

"Protein Structure and Topology"
Prof. Hiroaki Hiraoka (Kyushu University)

In this seminar, applications of computational homology to analysis of proteins were shown. In particular, compressibility of proteins was chosen as an example of structural properties, and it was successfully correlated with some topological properties such as robust "hole" in the protein modeled by van der Waals balls.

The lecturer used Homology groups as algebraic tools to study such geometrical "holes". In this framework, "simplicial complex" is given as an input data, and various geometrical properties such as connectivity (H_0), loop (H_1), cavity (H_2), n-dimensional hole (H_n) are obtained as outputs. Here, "simplicial complex" is a connection of tetrahedrons whose faces are shared by each other. They say pixel processing in computer graphics is similar to this transform to "simplicial complex".

He says that recent progress on computational homology allows us to easily treat them by using computers, and emphasizes that this approach is widely applicable to various targets, not only realistic objects but also abstracted ones including n-dimensional data structures. Some people seemed to be inspired to use it for analysis of the relation between structure and property in BMG systems. My approach to aqueous solution systems focusing on the structure of hydrogen-bond network can be sophisticated using this method. Indeed, abstraction of the topological structure from our research objects in materials science should be one of the helpful approaches to clarify the nature in them.

Report on the 6th Seminar

Susumu Tsukimoto

October 27, 2011

"Cantor sets meet the brain"

Prof. Ichiro Tsuda (Hokkaido University)

In this seminar, the talk were given by Prof. Tsuda who is an authority on chaos in complex systems and is recently studying on chaotic dynamics of the brain, entitled "Cantor sets meet the brain" and were followed by open discussions in order to have a clue for bridging between materials science and mathematics in WPI-AIMR.

Prof. Tsuda first introduced Libchaber's thesis which clearly described how a mathematical theorem takes part in an actual proof in laboratories. Then, he talked about the research example of this thesis, which is on a "mathematical model" for archicortex proposed to explain the formation of episodic memories in the brain base on the network structure of the hippocampus which provides fields for the creation of internal time connecting the past, present, and future. The theoretical model showing that the hippocampus plays a role in formation of dynamic memory via multiple time-scales interactions was presented in this seminar. He talked about the study with a similarity between the structures of hippocampal CA3 and CA1 and of two variables constructing a skinny baker's map, which is a typical two-dimensional chaotic map. The structure gave a hint to make a mathematical model of the hippocampus which is responsible for the formation of episodic memory. By correlating between experimental and mathematical studies of the network structures, chaotic behaviors were observed in hippocampal CA3, and also a Cantor set in hippocampal CA1. This example could suggest a promising relationship between mathematical and experiment studies of dynamic behavior in the brain science.

Following his talk, we organized open discussions, which were led by Dr. Tsukimoto. At first, Prof. Tanigaki asked a question on the experimental measurements of signals in neuron. In order to make effective collaborations between mathematics and materials science, Dr. Nakajima asked the speaker about possibility of Cantor set and/or other mathematical models to apply to materials science field as well as brain science.

Report on the 7th Seminar

Ken Nakajima

November 25, 2011

"Simulation study of a local glass transition temperature in polymer thin film"
Dr. Hiroshi Morita (AIST)

In this seminar, Dr. Morita introduced their study on a local glass transition and a polymer chain dynamics in polymeric materials using coarse-grained molecular dynamics (MD) simulation. According to his talk, the dynamics of the polymer chain in the confined geometry is different from that of the bulk, and these situations can be observed in many materials. Recently, Prof. Tanaka and co-workers in Kyushu University measured the glass transition temperature (T_g) near the substrate and it became larger as the analytical depth from the substrate became smaller and smaller. Furthermore, T_g of filler-contained polymeric materials were also measured by them and the feature of T_g was considered as a relation to T_g near the substrate. To clarify these problems, Dr. Morita conducted the coarse-grained MD simulation. He also briefly explained the coarse-graining technique and the simulation system of OCTA, which was developed by Prof. Masao Doi's group in The University of Tokyo, including Dr. Morita himself (http://octa.jp/).

After his talk, there were extensive questions and discussions. One arose from a researcher from the polymer group was the effect of the change in T_g to mechanical properties. This is actually important and we reached the conclusion that we need a further collaboration with Dr. Morita. A researcher in the BMG group put a question about the T_g change at surfaces. This is because it would be very interesting if this effect is also seen in BMG materials. Dr. Morita pointed out the possible parameters for this phenomenon. We will be able to study this point in the near future. Another question was the inhomogeneity recently observed in BMG and polymer surfaces by researchers in WPI-AIMR. He seemed to be interested in it. He will check his data in more detail in terms of inhomogeneity and will give us a report on it soon.

This time, he tried to talk the glass-transition phenomena as a generalized problem seen in many different types of materials and the audience agreed his point.

Nanomaterial Transport by Motor Proteins

Daniel Oliveira[1] and Winfried Teizer[1,2]

[1]WPI Advanced Institute for Materials Research, Tohoku University
[2]Department of Physics and Astronomy, Texas A&M University, College Station, TX, United States.

1. Introduction

Protein machines, also referred to as molecular motors, are the origin of nearly all biological movements within the eukaryotic cell. Conversion of chemical energy into mechanical work, harnessed by the hydrolysis of ATP, propels proteins' along cytoplasmic systems of fibers, such as microtubules. The kinesin protein (Figure 1) is a well known naturally occurring molecular machine capable of unidirectional cargo transport upon microtubule interaction, and consequently an attractive candidate as a constituent of a synthetic molecular machine. As illustrated in Figure 2, within the cytoskeletal network kinesin moves toward the (+)-terminus of microtubules (anterograde transport) having several functions including synapse activity [1,2].

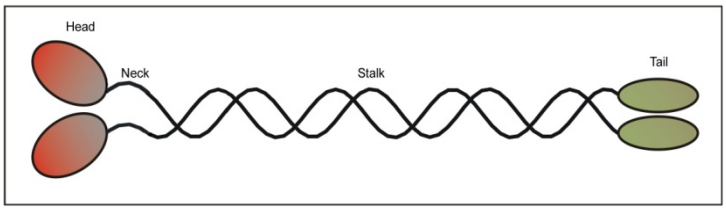

Figure 1. Kinesin dimer structure showing the heavy-chain (head domain) and the light-chain (tail domain).

Recent efforts to engineer tailor-made artificial nanotransport systems in order to carry out directional transport of nanoobjects in a cell-free environment are thus hardly surprising [3,4]. In a typical design, ATP-fueled kinesin motor proteins are immobilized on a glass surface while microtubules loaded with cargo are propelled over the motors. Alternatively, molecular shuttles can be assembled mimicking the natural cell`s intracellular transport mechanism where the kinesin protein moves over microtubules tracks (Figure 2). From a device engineering perspective, the latter approach for molecular shuttles is more appealing since multiple microtubules tracks with varying directions can be designed in the same device; moreover, bidirectional cargo transport can be achieved on the same track if different motor proteins are used (e.g., kinesin and dynein). Therefore, it is conceivable to utilize this concept for nanoelectromechanical systems. Kinesin motors have, in fact, been successfully used

for applications such as biomedical sensors [5], bio-molecular motion [6], and nanoparticle transport [7].

Relying on very strong and specific covalent interactions (e.g., biotin-avidin) kinesin can be coupled to functionalized nanocrystals, and accordingly, the interaction of such a complex with microtubules tracks can be visualized and investigated. It is therefore anticipated that molecular shuttles can be engineered by manipulating not only the cargo to be transported by kinesin but also the microtubule track network. This work is expected to develop novel opportunities for nanosize transport, especially for drug delivery.

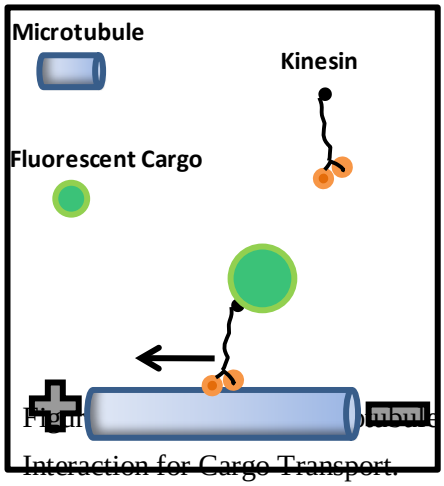

Figure 1. Microtubule Interaction for Cargo Transport.

2. Kinesin expression and kinesin-microtubule interaction observation

The first step toward the implementation of functional kinesin molecular shuttles is the construction, expression and purification of biotinylated kinesin dimers [8,9], currently performed in collaboration with Prof. Mitsuo Umetsu (WPI-AIMR at Tohoku University). Typically, the drosophila DNA fragment encoding the full-length kinesin heavy-chain motor domain is designed and modified by incorporating sequences of hexa-histidine and biotin tags. The recombinant kinesin protein is then expressed in Escherichia coli cells and purified by Ni-NTA chromatography. Following protein purification, the biotinylated recombinant kinesin protein is conjugated with streptavidin (or avidin) coated nanoparticles. Commercially available streptavidin-coated quantum dots (Invitrogen Corp.) are currently used for preliminary experiments on kinesin motility on microtubules. Microtubules (rhodamine-labeled) and fluorescent nanoparticles are then observed on an Olympus BX-51 fluorescence microscope, in collaboration with Prof. Tadafumi Adschiri (WPI-AIMR at Tohoku University).

3. Results and discussion

Two methods were used to quantify the relative amount of kinesin protein expressed in Escherichia coli, namely, sodium dodecyl sulfate polyacrylamide gel electrophoresis (SDS-PAGE), and Western Blot analysis of electrophoretic separated kinesin. Both methods rely on the electrophoretic separation of proteins based on their sizes, differing in how the sought protein is visualized. The later method estimates the molecular mass

of a protein by comparison with a protein standard, whereas in the former, protein visualization is achieved using fluorescent-labeled antibodies specific to the target protein (here, a his-tag antibody). Figure 3-A shows the SDS-PAGE result for the expressed kinesin heavy chain in Escherichia coli purified in a Ni Sepharose column and separated by size exclusion chromatography using a Superdex 200 column. Following electrophoresis, the polyacrylamide gel was stained with coomassie brilliant blue dye to allow visualization of separated protein bands, as seen in the figure. The first lane in the SDS-PAGE corresponds to the molecular weight marker (New England Biolabs), whereas lanes 2-10 are different Superdex 200 elution fractions. Since the designed kinesin protein has a molecular weight of 48 kDa, observation of Figure 3-A seems to indicate the presence of kinesin in fractions 2-10. Kinesin expression was supported by the Western Blot technique, where eluted fractions shown in Figure 3-A where detected with a fluorescent-labeled his-tag antibody (Santa Cruz Biotechnology). As illustrated in Figure 3-B, the kinesin protein was confirmed to be present in fractions 2-10.

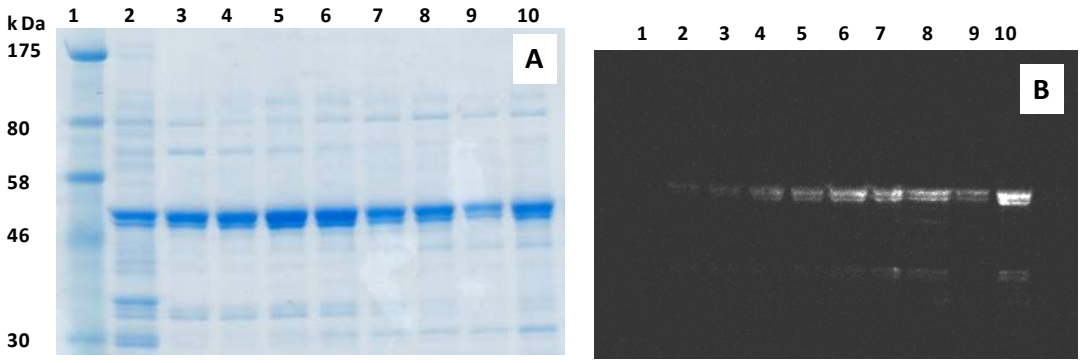

Figure 3. (A) SDS-PAGE: Lane 1, Molecular Marker; Lanes 2-10, Superdex 200 eluted fractions. (B) Western Blot with fluorescent labeled his-tag antibody: Lane 1, Molecular Marker; Lanes 2-10, Superdex 200 eluted fractions.

Following successful kinesin heavy chain preparation, the formation of microtubules was studied by controlling the polymerization of tubulin. A mixture of unlabelled tubulin and rhodamine-labelled tubulin was polymerized yielding stable fluorescent microtubules. Flow-cells constructed by the juxtaposition of KOH-cleaned cover slip and a microscope slide using double sided tape were used to observe microtubules with the fluorescent microscope. GTP (Guanosine-5'-Triphosphate) analogs are known to promote the polymerization of microtubules and also to prevent their depolymerization [10]; therefore, two GTP analogs where tested to study the difference, if any, in prepared fluorescent labeled microtubules, namely guanosine-5-[(,)-methyleno]

triphosphate, and guanosine-5'-monophosphate salts. It turns out that microtubules prepared with the latter salt are considerably longer than the ones prepared with the former salt. The reason for this is currently under investigation. Since the major components of the constructed nanotransport system are fluorescent (rhodamine-labelled microtubules for tracks and fluorescent quantum dots to be transported by kinesin), fluorescence microscopy is an elegant choice to visualize such systems. Microtubules shown in Figures 4-A and B were obtained after guanosine-5'-monophosphate salts polymerization, and microtubules on Figures 4-C and D were visualized after guanosine-5-[(,)-methyleno] triphosphate polymerization. A clear size difference in microtubules polymerized with the two distinct promoters can be easily observed by the corresponding fluorescence images.

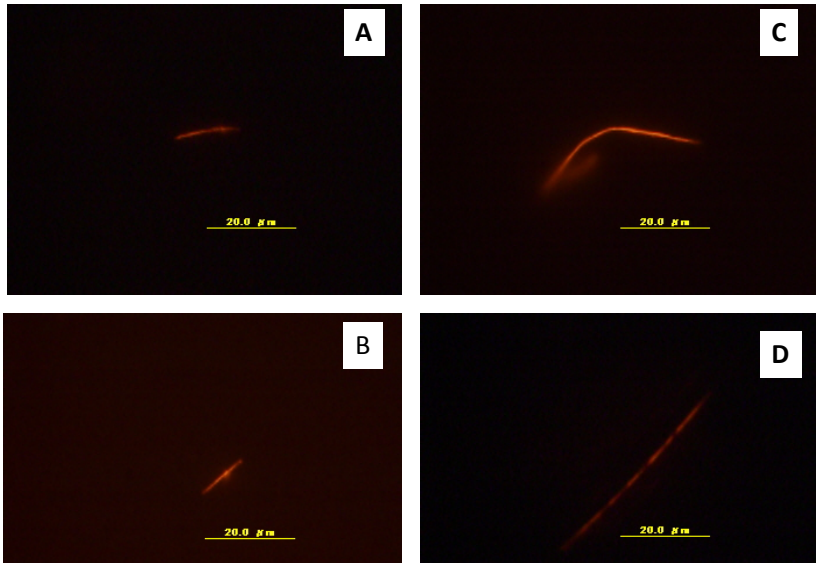

Figure 4. Microtubule fluorescent images. (A) and (B) microtubules polymerized in the presence of Guanosine-5'-monophosphate salts; (C) and (D) microtubules polymerized with Guanosine-5-[(,)-methyleno] triphosphate. Scale bar is 20 µm.

Following microtubule fluorescence observation, the kinesin-semiconductor nanocrystals complex, which consisted of biotinylated kinesin labeled with commercially available streptavidin-coated quantum dots (Qdot 605 nm, Invitrogen Corp), was assembled using a mixing ratio of 7 kinesin monomers per quantum dot. To visualize the kinesin-quantum dot conjugate interacting with the microtubule track, the

same procedure described in Figure 4 was followed except that after injecting the microtubule solution, the kinesin/quantum dot complex was flushed into the flow cell. Because of the linear motion observed, Figures 5 A-C are interpreted to show quantum dot motion along microtubules, where pictures A to C correspond to fluorescent time elapsed images collected every 500 ms, respectively. Due to equipment limitation, we are not able at the present time to unambiguously rule out other interpretations since no microtubules were directly observed near the quantum dots. Efforts are currently being made to overcome the problems in the fluorescent observation of kinesin-quantum dot conjugates by (1) using semiconductor nanocrystals with different emission wavelengths, (2) altering the length of microtubules, and (3) varying the ratio of kinesin to quantum dots. It should be noted that the fluorescence images shown in Figures 4 and 5 were obtained with a relatively low resolution system, coupled with a standard CCD camera (DP71). We are in fact currently assembling a state-of-the-art microscope at WPI-AIMR capable of providing the high level of precision and accuracy required for the direct observation of microtubules and more importantly, kinesin/nanoparticle complex motion on microtubules networks. Such a system, which is expected to be fully operational in September 2010, consists of an inverted fluorescence microscope (IX71, Olympus) equipped with a Total Internal Reflection condenser (IX2-RFAEVA, Olympus); evanescent illumination will be provided by the 488 nm line of an argon ion laser. Fluorescent images will be acquired with an electron multiplier charge couple device (ImageEM C9100-13, Hamamatsu). With this new instrument, we expect to be able to resolve and distinguish microtubules and quantum dots simultaneously.

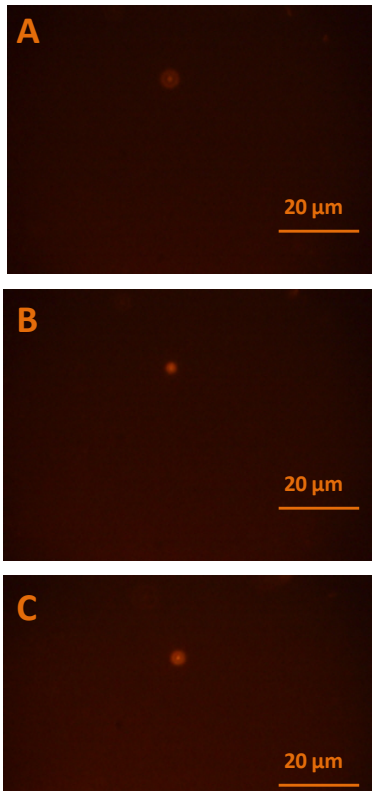

Figure 5. QD motion along microtubules. Images (A), (B) and (C) were collected with 500 ms intervals.

3. Summary

We have initiated an effort at WPI-AIMR in early 2010, which is aimed at understanding and constructing novel biomolecular systems for nanomaterials transport. Recombinant kinesin heavy chains have been expressed in Escherichia coli cells and

confirmed based on their molecular weight by SDS-PAGE and Western blot. In addition, microtubules networks were systematically polymerized and their length could be manipulated by controlling the addition of specific polymerizing promoter reagents. Furthermore, the artificially created kinesin proteins could be conjugated with fluorescent-labeled quantum dots and visualized by fluorescence microscopy. Deeper insight into such nanoscale transport systems will be achieved once the Total Internal Reflection Fluorescence (TIRF) microscope is fully operational, providing the high level of precision and accuracy required to the direct observation of such phenomena.

Acknowledgements

We acknowledge crucial support by our collaborators in the laboratories of Prof. Adschiri and Prof. Umetsu.

References

[1] A. Goel and V. Vogel *Nat. Nanotech.* **3**, 465-475 (2008).

[2] R. Dixit, J. L. Ross, Y. E. Goldman and E. L. F. Holzbaur *Science* **319**, 1086-1089 (2008).

[3] J. Noel, W. Teizer and W. Hwang *ACS Nano* **3**, 1938-1946 (2009).

[4] J. Noel, W. Teizer and W. Hwang *Journal of Visualized Experiments* **30**, (2009). http://www.jove.com/index/details.stp?id=1390

[5] T. Fischer, A. Agarwal and H. Hess *Nat. Nanotechnol.* **4**, 162-166 (2009).

[6] M. G. L. van den Heuvel and C. Dekker *Science* **317**, 333-336 (2007).

[7] R. K. Doot, H. Hess and V. Vogel *Soft Matter* **3**, 349-356 (2007).

[8] G. D. Bachand, S. B. Rivera, A. K. Boal, J. Gaudioso, J. Liu and B. C. Bunker *Nano Lett.* **4**, 817-821 (2004).

[9] D. L. Coy, M. Wagenbach and J. Howard *J. Biol. Chem.* **274**, 3667-3671 (1999).

[10] T. Mitchison and M. Kirschner *Nature* **312**, 237-242 (1984).

Engineering the Cellular Microenvironment

Hongkai Wu

WPI Advanced Institute for Materials Research, Tohoku University
Hong Kong University of Science and Technology, Hong Kong, P. R. China

Human physiology associates specific functions with each organ, for example, the liver acts as a filter for harmful substances contained within blood, it stores vitamins and minerals, and it produces cholesterol whereas the kidney filters blood and makes urine. These functions are specific to tissues even though the cells that make up tissues exhibit plasticity in their differentiated state. The earliest examples that exploit the instability of cells in tissues induced corneal epithelium to produce hair and transformed carcinoma cells into normal tissues (Figure 1) [1, 2]. These examples

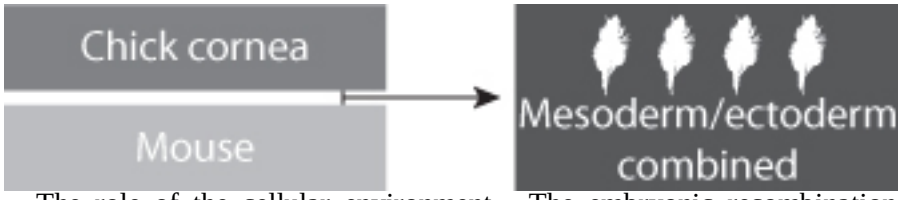

Figure 1. The role of the cellular environment. The embryonic recombination of mouse ectoderm with chick mesoderm produces an identity determined by the ectoderm; in this case,

indicated that the cellular microenvironment played an essential role in the function of cells.

Materials and Methods for Engineering the Cellular Microenvironment.

Researchers can create tissue-like microenvironments using tissue extracts or synthetic hydrogels. These materials include alginate, collagen [3], laminin-rich ECM [4], Matrigel (extracted from Engelbreth-Holm-Swarm mouse sarcoma), and photosensitive hydrogels [5]. The purpose of synthesizing and using biocompatible materials and fabricating ordered structures from these materials is to control the location of cells within the structured material. A suite of rapid prototyping tools developed under the heading of ‘soft lithography’ makes the patterning and control of liquids and polymers at the microscale possible [6]. Combining soft lithography with the natural and synthetic materials for cell culture presents intriguing possibilities for

controlling where cells grow in 3D, stimulating selective populations of cells, and engineering tissues from several types of cells.

Takeuchi et al. used an axisymmetric flow-focusing microfluidic device to fabricate hydrogel beads that contained cells [7]; the hydrogel beads self-assembled from a solution of peptides when exposed to ions. The combination of microfluidics, materials science, and cell biology exemplified in this work solved several problems for cell culture in 3D, namely, eliminating large chemical gradients that characterize millimeter-sized gels formed using conventional well plates and it simplified the preparation of beads that contain multiple types of cells. The same combination of microtechnology and biomaterials can provide control over the assembly of individual pieces of engineered tissue constructs. Sia et al. demonstrated the use of hydrogels that contain fibers of collagen that attach to neighboring hydrogels that contain fibers of collagen [8]. The ability to control how different and multiple phases of hydrogels interact at the molecular scale is likely to instruct the assembly of complex tissues using natural materials.

Several methods are available that produce aggregates of cells without using any material substitute for the ECM; these methods include suspending a drop of cells on an inverted substrate [9] and confining cells to chemically and topographically defined regions of a substrate (Figure 2) [10–12]. The design of micron sized tissues using

Figure 2. Substrates that contain topography cause cells to aggregate into spheroids. A pattern of adhesive (collagen) and non-adhesive (poly(ethylene glycol), PEG) regions are fabricated in a microwell using a stamp. Cells adhere selectively to the collagen and the

aggregates enables the size of the tissue to be controlled, which maximizes aggregate size and prevents oxygen and nutrient deficiencies within the aggregate; multiple types of cells can assemble in aggregates and organize among themselves; and, unlike microfluidics, the forces that cells experience during aggregation are unlikely to affect their function.

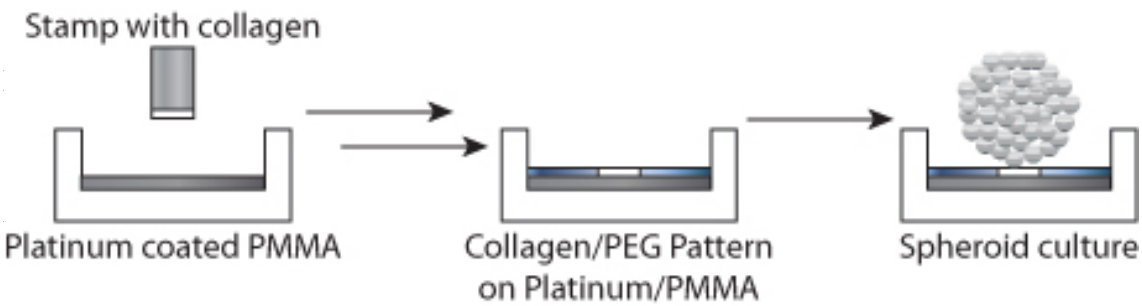

between cells cultured in 2D and 3D are distinct. In 3D, fibroblast cells exhibit

dendritic extensions or are bipolar and stellate (which morphology is observed is a function of how restrained and stiff the matrix is), however, on 2D substrata fibroblast cells are flat and are distinguished by stress fibers.

Bissell et al. developed a conceptual framework for thinking about the relationship between cells and their microenvironment using breast cancer as a model system [13, 14]. One of several outcomes from this framework was evidence that 3D cell culture models can be used to identify functional genes and proteins and validate targets for therapy. For example, the ß1-integrin receptor mediates cell-extracellular matrix interactions and increased expression of ß1-integrin correlated with poor survival in patients, however, down-modulation of ß1-integrin results in reversion of the malignant phenotype by arresting growth and restoring tissue polarity when propagated in a 3D microenvironment. Addition of ß1-integrin inhibitory antibody to tumor cells cultured in laminin-rich ECM gels decreased the rate of proliferation and numbers of cells and increased apoptosis.

The relationship between, for example, fibroblasts and collagen matrix is reciprocal: fibroblast cells remodel the matrix, which increases the tension within the matrix, which feeds back into the cells and alters the mechanisms that are used to further remodel the matrix. Primary hepatocytes, when cultured on collagen or basement membrane proteins, assume their differentiated shape and they express high levels of mRNA for liver-specific genes [15]; in contrast, the same cells cultured on plastic substrata exhibit a dedifferentiated, flattened shape, because the substratum is inelastic; liver-specific gene transcription also declines dramatically on flat substrata.

Aggregates of cells can be used to produce protein therapeutics in quantities several times greater than the amounts produced by suspended cells in protein-free media, however, it is unclear if this phenomenon can scale to compete with bioprocesses that are currently used for production of proteins [9].

Our Research Program.

Our lab focuses on problems that exist at the interface of microfabrication, materials science, microscopy, and cell biology and range from manipulating individual cells to organizing thousands of cells. We demonstrated the fabrication of monodispersed alginate gels that contained cells using biocompatible polymer membranes (Figure 3) [16] and we developed methods that modify the most popular material for microfluidics research (poly(dimethylsiloxane), PDMS) with fluorescent

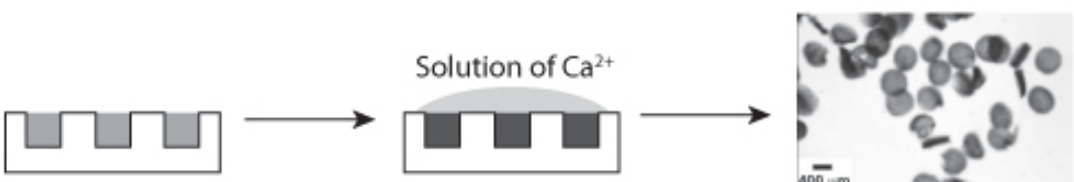

quantum dots for sensitive readout of temperature in microchannels [17] and with paraffin wax, which rendered PDMS airtight [18].

Our recent work uses topographically defined substrates to create spheroid cultures of cells and organizes multiple types of cells cultured in collagen gels. These projects are part of our continuing efforts to demonstrate the simplest methods that can culture cells in their natural environments and to characterize their behavior using accessible microscopy tools. We expect the outcome of our efforts to define methods that provide appropriate metabolites and nutrients for each type of cell in a multicellular engineered tissue.

References.

[1] JL Coulombre and Coulombre A.J. *Dev. Biol.* **25**, 464 (1971).
[2] C. Ferraris, C. Chaloin-Dufau, and Dhouailly D. *Differentiation* **57**, 89 (1994).
[3] R.B. Vernon and Gooden M.D. *In Vitro Cell. Dev. Biol.* **38**, 97 (2002).
[4] N. Boudreau, C. Myers, Bissell M.J. *Trends Cell Biol.* **5**, 1 (1995).
[5] Hubbell J.A. *Curr. Opin. Biotech.* **14**, 551 (2003) and references therein.
[6] Y. Xia and Whitesides G.M. *Angew. Chem., Int. Ed.* **37**, 550 (1998).
[7] Y. Tsuda, Y. Morimoto and Takeuchi S. *Langmuir.* **26**, 2645 (2009).
[8] B.M. Gillette, J.A. Jensen, B. Tang, G.J. Yang, A. Bazargan-Lari, M. Zhong and Sia S.K. *Nat. Materials.* **7**, 636 (2008).
[9] J.M. Kelm and Fussenegger M. *Trends Biotech.* **22**, 195 (2004).
[10] J. Fukuda, Y. Sakai and Nakazawa K. *Biomat.* **27**, 1061 (2006).
[11] D.M. Dean, A.P. Napolitano, J. Youssef and Morgan J.R. *FASEB J.* **21**, 4005 (2007).
[12] A.P. Napolitano, P. Chai, D.M. Dean and Morgan J.R. *Tissue Eng.* **13**, 2087 (2007).

Figure 3. Fabrication of individual pieces of hydrogel that contain bacterial cells using a microfabricated membrane. PDMS wells pattern the location and geometry of a solution of alginate, which is converted to a gel when exposed to a solution of divalent ions, for example,

[13] H. Liu, D.C. Radisky, F. Wang and Bissell M.J. *J. Cell Biol.* **164**, 603 (2004).
[14] C.C. Park, H. Zhang, M. Pallavicini, J.W. Gray, F. Baehner, C.J. Park et al. *Cancer Res.* **66**, 1526 (2006).
[15] C.M. DiPersio, D. Jackson and Zaret K.S. *Mol. Cell. Biol.* **11**, 4405 (1991).

[16] C. Qiu, M. Chen, H. Yan and Wu H.K. *Adv. Mater.* **19**, 1603 (2007).
[17] J.H. Zhou, H. Yan, Y.Z. Zheng and Wu H.K. *Adv. Func. Mater.* **19**, 324 (2009).
[18] K.N. Ren, Y.H. Zhao, J. Su, D. Ryan and Wu H.K. *Anal. Chem.* **82**, 5965 (2010).

Development of Novel Methods of Surface Forces Measurement for Nano-Materials Science

Kazue Kurihara

WPI Advanced Institute for Materials Research & IMRAM, Tohoku University,
Katahira, Aoba-ku, Sendai 980-8577, Japan
E-mail: kurihara@tagen.tohoku.ac.jp

1. Introduction

One of important challenges in advanced materials science is bridging a gap between materials nano-science and real materials, that is, designing real materials in nano-scale precision like biological systems. In order to achieve this goal, it is essential to elucidate and regulate molecular and surface interactions. Self-assembly is essential at all scales in biology, which demonstrates an ideal model for designing materials at the atomic and/or molecular level of precision.

Surface forces measurement and atomic force microscopy (AFM) have made it possible to directly measure molecular and surface interactions in liquids as a function of the surface separation with high sensitivity. Naturally, they have become powerful tools for studying the origins of forces operating between molecules and/or surfaces of interest [1, 2]. They also offer a unique, novel surface characterization method, which "monitors surface properties changing from the surface to the bulk (depth profiles)" and provides new insights into surface phenomena [3]. This method is direct and simple. It is difficult to obtain a similar depth profile by other methods; X-ray and neutron scattering measurements can provide similar information but require extensive instrumentation and appropriate analytical models.

Our research concerns "elucidation of molecular and surface interactions as well as surface properties of nano-materials", and "development of novel functionalized molecular architectures". For this purpose, we use the surface forces measurement as a major tool. Molecular architectures are self-organized polymolecular systems where molecular interactions play important roles. They exhibit specific and unique functions that could not be afforded by single molecules. Molecular architecture chemistry beyond molecules is not only gaining a central position in chemistry but becoming an important interdisciplinary field of science [4]. Recently, the concept has extended to architectures of nano-scopic objects such as nano-particles and nano-rods [5]. Investigation of molecular architectures by surface forces measurement is important from the following points of view.

(1) It is essential to elucidate intermolecular and surface interactions involved in self-organization, of which significance is not limited to material science but extends to the ingenuity of biological systems.

(2) The importance of surface characterization in molecular architecture chemistry and engineering is obvious since solid surfaces are becoming essential building blocks for constructing molecular architectures as demonstrated in self-assembled monolayer formation and alternate layer-by-layer adsorption [6], and assembles of nano-particls [5]. Surface-induced structuring of liquids is also well-known [7, 8], which bears implications for micro- and nano-technologies (i.e., liquid crystal displays and micromachines). Because surface forces are sensitive to change in surface force characteristics, force measurement could point out intriguing phenomena. For example, we found novel molecular architecture (alcohol macroclusters) at solid –liquid interfaces [9, 10].

(3) Two-dimensionally organized molecular architectures can be used to simplify the complexities of three-dimensional solutions and allow the surface forces measurement. By employing this approach, we can study complex systems such as polypeptides and polyelectrolytes in solutions [11], and specific interactions of proteins [12].

Earlier studies of surface forces measurement were mainly concerned with surface interactions determining the colloidal stability including surfactant assemblies [1, 2]. It has been demonstrated, however, that a “force-distance” curve can provide much richer information on surface molecules; thus it should be utilized for studying a wider range of phenomena [13]. Practically, the preparations of well-defined surfaces, mostly modified by two-dimensional organized molecules, and the characterization of the surfaces by complementary techniques are keys to this approach. A similar concept is “force spectroscopy” [14], coined to address force as a new parameter for monitoring the properties of materials. A major interest in force spectroscopy is the single molecular measurement generally employing an atomic force microscope [15]. On the other hand, the forces measurement of two-dimensionally organized molecules has advantages complementary to those of single molecule force spectroscopy. It can monitor many molecules at the same time and thus is better suited for studying long-range weaker forces. The measurement should bear a close relevance to real systems that consist of many molecules, because interactions between multiple molecules and/or macroscopic surfaces in solvents may exhibit characteristics different from those between single molecules. The surface forces measurement possesses its own virtue.

In spite of its obvious importance, the surface forces measurement remained a

relatively specific tool in the field of colloid and interface science. A major drawback of surface forces measurement employing surface forces apparatus (SFA) is restriction of samples: it is applicable only for transparent substrates and liquids because it uses FECO fringes for the distance determination [1]. We have recently developed a novel SFA, a twin-path SFA (Figure 1), which is a practically only SFA for opaque samples [16].

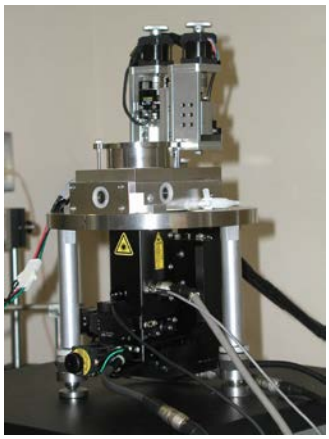

Figure 1. Photograph of a major part of the twin-path SFA.

Another instrumentation we have involved is the shear force measurements. Taking an advantage from an ability of the surface forces apparatus to regulate the surface separation with a high resolution, various shear measurements have been developed to study confined liquids. This paper describes the resonance shear measurements (RSM) which we have also recently developed [17]. Using this measurement, it is possible to perform measurement for nano-rheology and nano-tribology.

2. Experimental Section

2.1 Twin-path Surface Forces Apparatus (Twin-path SFA)

A schematic diagram of the twin-path SFA is shown in Figure 2. The top surface is fixed to the stainless steel chamber and the bottom surface is mounted on a double-cantilever spring supported by a shaft connected to the surface drive system. The distance between surfaces was mechanically controlled by the drive system composed of a pulse motor (Oriental Motor Co., Ltd.) in combination with the differential spring. The displacement of the bottom surface was measured using the twin-path distance measurement unit.

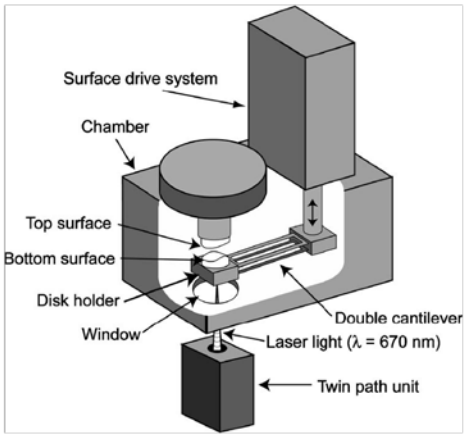

Figure 2. Schematic diagram of the twin path SFA. Laser light (λ = 670 nm) goes through the window at the bottom of chamber and is reflected by the back of the disk holder. The reflected light is monitored by the twin path unit. The surface distance is controlled by a surface drive system.

The mica surfaces glued on silica lenses were mounted in the SFA chamber, and the distance between them was measured by FECO (Fronges of Equal Chromatic Order) using the common procedure [1]. The lower surface was driven by a certain number of counts and the change in the distance was determined. The displacement/pulse thus determined was 0.0050 ± 0.0002 nm in the working range of 4 μm.

The detail description of the twin path unit is shown in Figure 3. The collimated light beam emitted from a laser diode (λ = 670 nm) (Applied Techno Corp.), was split into several orders of interferometric light by a diffraction grating. The +1st order diffracted light was entered to the SFA chamber from the bottom window and reflected by the mirror of the lower sample holder, while the –1st order diffracted light is reflected by the fixed mirrors in the twin path unit. These reflected lights are recombined with each other on the four diffraction gratings attached to the four-sectored photo diode (Hamamatsu Photonics K. K.). The different intensities of the interference pattern with the phase shift of 0, 90, 180, 270 degrees were detected by the four-sectored photo diode (Figure 4). The phase difference between the ± 1st order lights is calculated using the following équation[18],

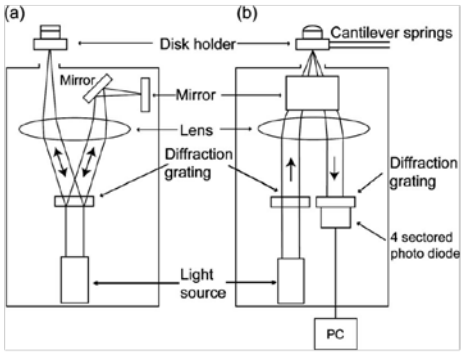

Figure 3. Schematic figures of the twin path distance measurement unit ((a) front view and (b) side view). The +1st and –1st order beams are reflected by the bottom of the disk holder and that by the fixed mirrors, respectively and are recombined on the diffraction grating. The recombined beam is detected by the 4-sectored photo diode and analyzed by the PC.

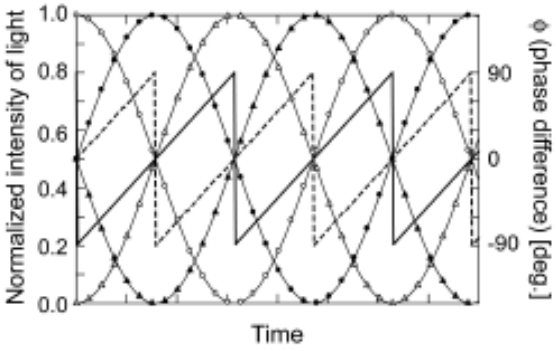

Figure 4. Schematic figure of the changes in the intensities of laser light (CH1, solid circles; CH2, open circles; CH3, solid triangles; CH4, open triangles) and obtained phase differences shown as jagged curves (ϕ_1 , solid line; ϕ_2 , broken line) on approach.

$$\phi_1 = \arctan\{(I_4 - I_2)/(I_1 - I_3)\} \qquad (1)$$

where ϕ_1 is the phase difference (degree) and I_1, I_2, I_3, and I_4 are the intensities of the light recorded by Channel 1 (CH1), 2 (CH2), 3 (CH3), and 4 (CH4) of the four-sectored photo diode, respectively. This phase difference shows the jagged curve with the change in the surface displacement as shown in Figure 3. The surface displacement, D (nm), can be obtained from the équation [18],

$$D = \frac{1}{2}\frac{\phi_1}{360} \times \lambda \qquad (2)$$

where λ is the wavelength of laser light (λ = 670 nm).

The resolution of the surface displacement would be low at the steep gradient parts of ϕ_1 as shown in Figure 3. To avoid this problem, we calculate simultaneously the phase difference, ϕ_2, by equation (3),

$$\phi_2 = \arctan\{(I_3 - I_1)/(I_4 - I_2)\} \qquad (3)$$

to replace ϕ_1 in equation (2), when the ϕ_1 is in steep gradient parts.

2.2 Resonance Shear Measurement (RSM)

A photograph and a schematic drawing of the device for resonance shear measurement are shown in Figure 5. The droplet of a liquid was confined between upper and lower solid (typically mica or silica) surfaces. The upper surface was laterally oscillated with various frequencies by applying the sinusoidal voltage (U_{in} and $-U_{in}$) to the two opposite electrodes of the four-sectored piezo tube. The movement of the upper surface is monitored by the capacitance probe, and the output voltage (U_{out}) was plotted as the amplitude ratio of U_{out} /U_{in} as a function of frequency. This is the shear resonance curve, which shows the maximum amplitude at a characteristic (resonance) frequency. When the upper and lower surfaces are in a large separation, the height of this resonance peak is sensitive to

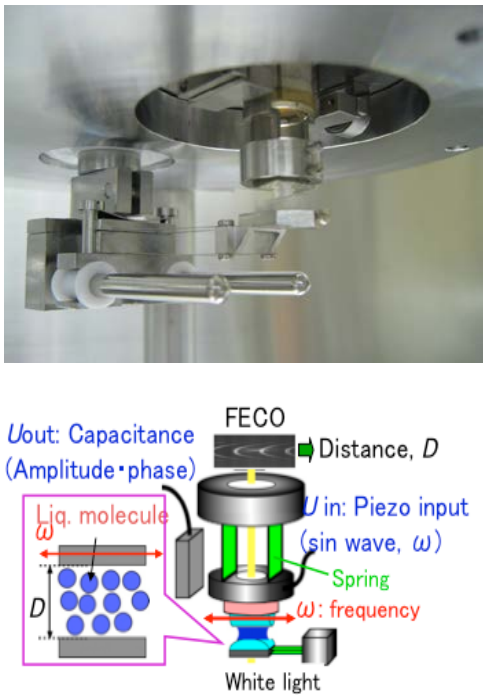

Figure 5. The device for resonance shear measurement : a photograph (top) and a schematic drawing (bottom).

the viscosity of confined liquid and decreases with decreasing the surface separation. When the surfaces come closer, the resonance frequency usually shifts to a higher frequency due to the coupling of the upper and lower surfaces mediated by confined liquid (due to the contribution of the spring of the lower unit).

3. Results and discussion

3.1 Linearity and Resolution of Distance Determination by Twin-path SFA

We first examined the linearity in the displacement measurement by the twin path unit for large displacement range. The movement of a mirror fixed at the end of the surface drive unit was measured by both of a capacitance probe (ST-0535A, IWATSU Electric Co., Ltd.) and the twin path unit. The surface drive unit was operated by a pulsed motor with a differential spring (see Figure 2). The displacement measured by the twin path unit and by the capacitance probe well agreed with the calculated value using the data (0.008 nm/pulse by FECO for this drive system). The deviations between the measured and the calculated values were ca. 2% for twin-path method and 4% for capacitance probe over the 5 μm, respectively. The measurements by the twin path unit showed higher accuracy and linearity than the capacitance probe used in this study.

In order to examine the resolution of displacement measurement by the twin path method, the stepwise motion of mirror was given by the pulse motor was monitored. The mirror surface was moved by 1 nm (pulse counts, 200; velocity, 400 counts/s) every 5 seconds interval and the total displacement was measured every second. Figure 6 plots the data at every second together with the calculated value based on the given pulses. The measured data agreed well with the estimated value, and the resolution of a current set-up is 0.2 nm, which is close to the resolution by FECO (0.1 nm).

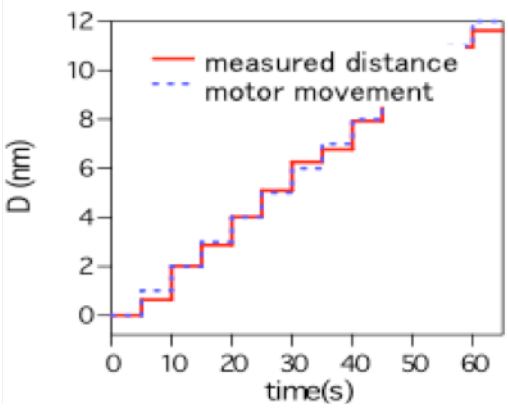

Figure 6. The displacements in air measured by the twin path method (solid line) compared with the calculated value from the pulse number of motor (dotted line).

3.2 Double Layer Force between Mica Surfaces Measured by Twin-path SFA

In order to demonstrate the reliability of the apparatus, we performed typical

measurements. The surface forces between mica surfaces in aqueous KBr (MERCK, suprapur) (0.1 mM, 1.0 mM and 10.0 mM) were measured by injecting the KBr solution into the chamber. These surface force profiles are plotted in Figure 7. The decay lengths of 32 ± 3 nm, 11 ± 1 nm, 4 ± 1 nm for 0.1 mM, 1.0 mM and 10.0 mM, respectively, were well agreement with the theoretical Debye lengths (30.4 nm, 9.6 nm, 3.0 nm) [1]. The broken lines indicated the theoretical fits to DLVO forces of the constant surface potential (0.1 mM, 90 mV; 1.0 mM, 90 mV; 10.0 mM, 50 mV) and constant surface charge (0.1 mM, 0.02 charge/nm^2; 1.0 mM, 0.06 charge/nm^2; 10.0 mM, 0.08 charge/nm^2) conditions. The pull-off force was detected only in 0.1 mM KBr solution as 2.6 ± 1.6 mN/m. These results are well agreement with previous results measured by the conventional SFA[1,2].

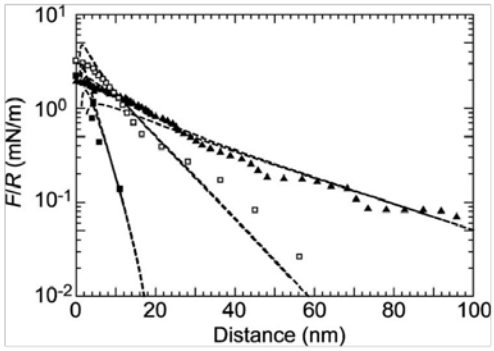

Figure 7. Surface forces between mica surfaces in aqueous KBr solution. The solid triangles, open squares, and solid squares are the profiles of 0.1 mM, 1.0 mM and 10.0 mM KBr solutions. The broken lines denote the theoretical DLVO curves at constant surface potential and constant surface charge conditions.

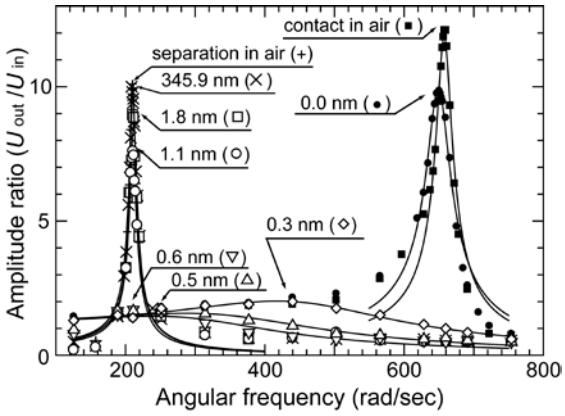

Figure 8. Resonance curves for NaCl solution (7 mM) confined between mica surfaces at seven distances: 345.9 nm, 1.8 ± 0.3 nm (load = 0.14 mN), 1.1 ± 0.3 nm (0.24 mN), 0.6 ± 0.3 nm (0.55 mN), **0**.5 ± 0.2 nm (1.33 mN), 0.3 ± 0.2 nm (2.15 mN), 0.0 ± 0.3 nm. The reference states of the separation and mica-mica contact in air are shown together. The arrows denote the peak position of the resonance curve at the surface distances. The solid lines denote the fitting curve**s** to our mechanical model.

3.3 Aqueous NaCl Solution Confined between Mica Surfaces Measured by RSM.

The dynamics of confined water thinner than a few nanometers were in controversial in previous studies [19, 20]. Our study employing RSM provided a

comprehensive picture for this complicated situation[21]. The viscoelasticity of the thin film of aqueous NaCl solution confined between mica surfaces was measured by shear resonance apparatus. The observed shear resonance curves (Figure 8) at separations less than ca. 2 nm indicated that the solution exhibits the high lubrication effects under some loads. The distances were measured using FECO. The effective viscosity (0:1–10 Pa s) obtained for the separations less than 1 nm from a mechanical model was 2 – 4 orders of magnitude larger than the bulk value.

3.4 Ionic LIquids Confined between Silica Surfaces Measured by RSM.

Recently, we applied RSM for ionic liquids. Two types of imidazolium-based ionic liquid (IL), 1-butyl-3-methylimidazolium bis(trifluoromethanesulfonyl)amide ([C_4mim][NTf_2]) and 1-butyl-3-methylimidazolium tetrafluoro borate ([C_4mim][BF_4]), confined between silica surfaces were investigated by RSM together with surface force measurement [22]. The surface force profiles in the ILs showed oscillatory solvation forces below the characteristic surface separations: 10.0 nm for [C_4mim][NTf_2] and 6.9 nm for [C_4mim][BF_4]. The more pronounced solvation force found in [C_4mim][NTf_2] suggests that the crystalline property of the IL contributes to the stronger layering of the Ils adjacent to the surface. The resonance shear measurement (Figure 9) and the physical model analysis revealed that the viscosities of the confined Ils were 1−3 orders of magnitude higher than that of the

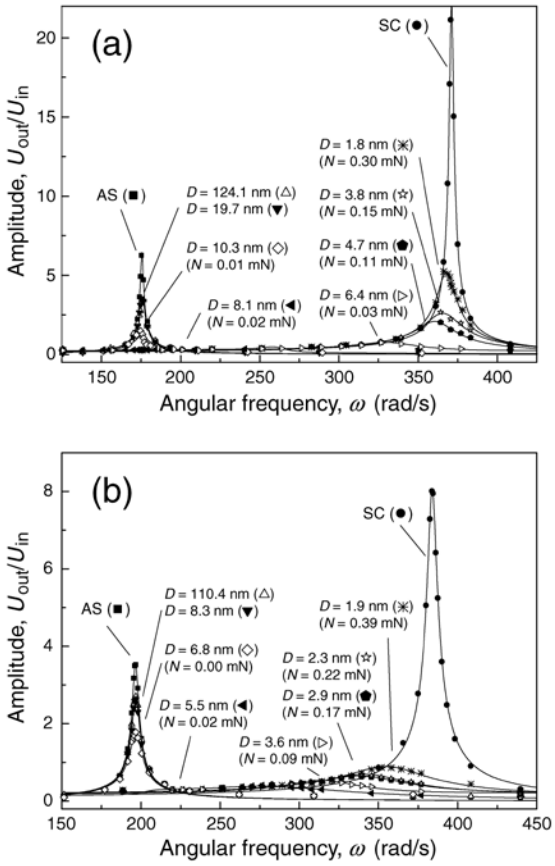

Figure 9. Resonance curves for (a) [C_4mim][NTf_2] and (b) [C_4mim][BF_4] confined between silica surfaces at various separation distances under applied load *N*. Reference curves for separated in air (AS) and connected by silica-silica contact (SC) are also shown. Solid lines denote the best fitting curves on the basis of a physical model [23].

bulk IL. This study also focused on the correlation between the resonance shear behaviour and the lubrication property of the Ils, and the suspension rheology in the Ils. An understanding of the solid-IL interface and of Ils confined in nanospace will facilitate the further development of novel applications employing Ils.

4. Conclusion

This paper reviews a new surface forces apparatus (twin-path SFA) and resonance shear measurement, both we have developed recently. With the twin-path SFA, it is possible to use metals, ceramics and other opaque samples for substrates. They are not only interesting materials but provide opportunities for broader applications of the forces measurement: for example, we have constructed electrochemical SFA using gold as electrodes [24]. The twin-path SFA is compact compared with the conventional SFA using FECO, and easily operated by a computer. Combining with a spectroscope, spectroscopic SFA for fluorescence lifetime measurement was developed [25].

The properties of confined liquids are different from those of the bulk due to the confinement effect and the interaction of liquid molecules with the surfaces. They attract increasing attention because of recent progress in the preparation of many porous materials including nanotubes and the nano-fabrication processes such as nanoprinting [25]. Shear measurement based on SFA can offer a useful tool for studying confined liquids. Especially, the resonance method is relatively easy to operate, and applicable for both nano-rheology and –tribpology. Resonance responses are sensitive to changes in properties of confined liquids, so it is possible to monitor changes in viscosity, traction and triblogical properties, and even stick-slip phenomena, which are often correlated with structural and/or packing properties of liquids. We expect these measurements will be more widely used in material science.

References

[1] J. Israelachivili, Intermolecular and Surface forces 3rd ed., (2011).

[2] A. W. Adamson, A. P. Gast. Physical Chemistry of Surfaces 6th ed. New York: John Willy& Sons (1997).

[3] K. Kurihara, Nano-Surface Chemistry M. Rosoff ed., Marcel Dekker Inc., 1 (2002).

[4] J.-M. Lehn, Supramolecular Chemistry, Weinheim: VCH (1995).

[5] D. V. Talapin, J.-S. Lee, M. V. Kovalenko, E. V. Shevchenko, Chem. Rev. **110**, 389 (2010).

[6] G. Decher, Science **277**, 1232 (1997).

[7] J. Israelachvili, H. Wennerstrom, Nature **379**, 219 (1996).
[8] G. Reiter, A. L. Demiral, S. Granick, Science **263**, 1741 (1994).
[9] M. Mizukami, K. Kurihara, Chem. Lett. **28**, 1005 (1999); ibid. **29**, 256 (2000).
[10] M. Mizukami, M. Moteki, K, Kurihara, J. Am. Chem. Soc, **124**, 12889 (2002).
[11] T. Abe, K. Kurihara, N. Higashi, M. Niwa, J. Phys. Chem. **99**, 1820 (1995).
[12] T. Suzuki, Y.-W. Zhang, T. Koyama, D. Y. Sasaki, K. Kurihara, J. Am. Chem. Soc. **128**, 15209 (2006).
[13] K. Kurihara, Adv. Colloid Sci. **71-72**, 243 (1997).
[14] N. A. Burnham, R. J. Colton. In: D. A. Bonnel, ed. Scanning Tunneling Microscopy and Spectroscopy. New York: VCH, 191 (1993).
[15] G. V. Lee, L. A. Chrisey, R. J. Colton, Science **266**, 771 (1994).
[16] H. Kawai, H. Sakuma, M. Mizukami, T. Abe, Y. Fukao, H. Tajima, K. Kurihara, Rev. Sci. Instrum. **79**, 043701 (2008).
[17] C. Dushkin, K. Kurihara, Rev. Sci. Instrum. 69, 2095(1998).
[18] K. Creath, in Progress in Optics (Ed. by E. Wolf), Elsevier Science Publishers B. V., **26**, 349 (1988).
[19] Y. Zhu and S. Granick, Phys. Rev. Lett. **87**, 96104 (2001).
[20] U. Raviv and J. Klein, Science **297**, 1540 (2002).
[21] H. Sakuma, K. Otsuki, K. Kurihara, Phys. Rev. Lett. **96**, 046104 (2006).
[22] K. Ueno, M. Kasuya, M. Watanabe, M. Mizukami and K. Kurihara, Phys. Chem. Chem. Phys. **12**, 4066 (2010).
[23] M. Mizukami and K. Kurihara, Rev. Sci. Instrum. **79**, 113705(2008).
[24] T Kamijo, M. Kasuya, M. Mizukami and K. Kurihara, Chem. Lett., **40,** 674 (2011) .
[25] D. Fukushi, M. Kasuya, H. Sakuma and K. Kurihara, Chem. Lett. **40,** 776 (2011) .

Bioelectrochemical Imaging with Micro/Nanoelectrode Systems

Tomokazu Matsue[1,2], Kosuke Ino[2], Yasufumi Takahashi[2,3], Andrew I. Shevchuk[3], Pavel Novak[3], Yuri E. Korchev[3] and Hitoshi Shiku[1,2]

[1] WPI Advanced Institute for Materials Research, Tohoku University, Sendai 980-8579, Japan

[2]Graduate School of Environmental Studies, Tohoku University, Sendai 980-8579, Japan

[3]Division of Medicine, Imperial College London, Hammersmith Hospital Campus, London, W12 0NN, United Kingdom

1. Introduction

Recently, the development of multipoint measurements and imaging of biomaterials has received a great deal of attention due to the strong demand for rapid, comprehensive, and high-throughput analyses. These techniques allow simultaneous detection and quantification of multiple analytes. A variety of array-based biosensing systems have been developed so far. Most of them are based on fluorescence detection or imaging because fluorescence measurements typically have high sensitivity and a variety of tools for performing the measurements is commercially available. However, fluorescence detection has some disadvantages, such as undesired fluctuations due to quenching or emission from non-target materials, shielding by turbid solution, and the need to label non-fluorescent species, which may cause toxic side effects during analyses. As an alternative method, electrochemical detection or imaging has also been applied for detailed analysis of biomaterials. Array-based electrochemical devices have also been used for multipoint measurements. The electrochemical signal can be processed by conventional electronics in a very cheap and fast manner. Furthermore, miniaturized electrochemical transducers can easily be integrated in a microsystem by employing conventional microfabrication technologies. In the past decade, various types of amperometric microelectrode arrays for multipoint measurements and bioimaging have been designed and applied to chemical and biological analyses. These electrochemical array devices have substantial advantages, including rapid response time and qualitative and quantitative detection. Scanning electrochemical microscopy (SECM) is also a popular electrochemical imaging system [2]. SECM uses a micro/nanoelectrode as a scanning probe and provides sample surface electrochemical property under physiological conditions without physical contact. Because of unique properties SECM has been applied localized electrochemical measurements.

In this article, we will describe the recent progresses of electrochemical measurements and bioimaging with integrated micro/nanoelectrde devices. Bioimaging with scanning electrochemical microroscopy (SECM) with a micro/nanoelectrode probe will also be reported.

2. Adderable measurement with micro/nanoelectrode devices

Among the various electrochemical arrays, the development of an individually addressable device for multipoint measurements and bioimaging has been recognized as a key issue to cope with increasing demands for a versatile, reliable and easy-to-use analytical system, especially for comprehensive screening purposes. However, it is difficult to collect electrochemical responses at many individual measurement points using a conventional electrochemical device, because sufficient space for the bond pads is not available on the chip border. To solve this problem, we have proposed a novel method to realize individually addressable electrochemical measurement using a device consisting of two sets of microelectrode arrays.

In the device, column and row electrodes were orthogonally arranged on two different glass substrates in order to assemble an addressable microelectrode device for the purpose of comprehensive electrochemical detection [3]. An amperometric signal was separately detected at the individual crossing points of the column and row electrodes on the basis of redox cycling of localized electroactive species occurring between the electrodes. The addressable microelectrode device was simple and could be easily assembled; however, it comprised as many as 10 × 10 addressable detection points on a single chip. The basic electrochemical performance of the device was investigated by using the ferricyanide/ferrocyanide redox couple. Electrochemical responses at 100 individual points could be collected within 22 s. The present device was successfully used for imaging the spots of alkaline phosphatase on the array substrate. The results indicate that the device can be applied to comprehensive and high-throughput detection and imaging of biochemical species.

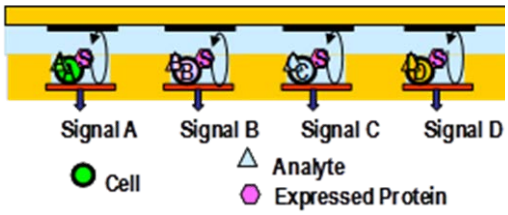

Fig. 1. Principle an addressable microelectrode / microwell array for comprehensive electrochemical analysis.

A microwell array was further incorporated into the addressable device to conduct high-throughput screening of bioparticles and genetically engineered cells

accommodated in the wells [4]. We demonstrate the rapid electrochemical detection of the reporter protein—secreted alkaline phosphatase (SEAP)—from a single genetically engineered HeLa cell (HeLa-pSEAP) using the addressable microelectrode/microwell array device. Figure 1 shows the operation principle of detection of the reporter protein with the addressable device. The HeLa-pSEAP cells that secrete ALP were randomly seeded in the microwells and the amplified current was detected. The reduction current for the microwell with a single HeLa-pSEAP cell increased with time, while no meaningful response was detected for the empty wells. These results indicate that SEAP secreted from the cell catalyzes the hydrolysis of PAPP to produce PAP, which is accumulated in the well.

Figure 2 shows an image of the reduction current of each microwell after 20 min of incubation time. The responses in the empty microwell is 0.754 ± 0.996 pA while in cell occupied microwell is 16.3 ± 5.49 pA. Figure 2(c) shows histogram of the current responses distribution from the cells, unlike the case for ALP beads, each single HeLa-pSEAP cell showed a different current response, approximately 20 % of the cells show responses similar to those observed for wild-type cells. These variations in the response are due to the different expression levels of ALP from individual cells and the size variations of single cells. The average amount of PAP generated from the catalytic reaction of a single HeLa-pSEAP cell was calculated from the current responses and found to be 3.6 × 10–17 mol for an incubation time of 20 min. These results demonstrate that the present device can be used for highly sensitive and high-throughput screening to detect the protein expression activity of genetically engineered cells at the single-cell level. Since the ALP has been widely used as a labeling enzyme and reporter protein, the present device can be used for the screening of a

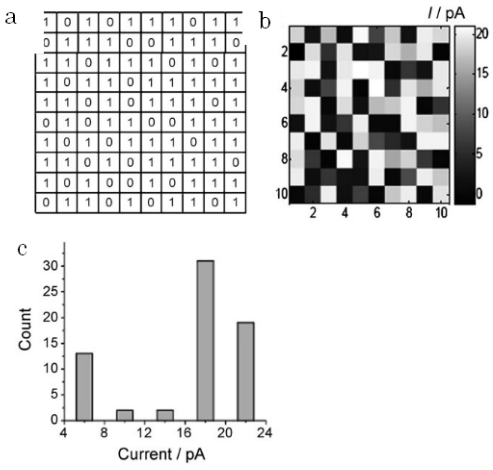

Fig. 2. a) Scheme of cells in the microwells. The number represents the number of cells in each well. b) Imaging of the current responses at 10x10 microwells. This image was taken 20 min after the injection of PAPP. c) Histogram of the current response distribution of the cells.

comprehensive analysis of DNA, proteins, and cells [5].

3. Bioimaging with micro/nanoelectrode devices

Although the device described above is very useful for high-throughput electrochemical detection, careful assembly of the device is required to align two different glass substrates with the row or column electrodes at exact locations upon each measurement, which is time-consuming and results in low reproducibility. Furthermore, there is no open space on the device for handling samples such as cells, because the sensor areas are surrounded by glass substrates with electrodes. In this study, we have developed a new device to solve these problems.

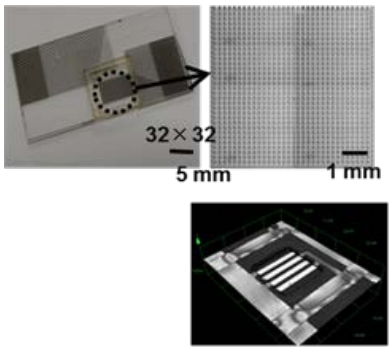

Fig. 3. Images of the 32 × 32 crossing points and the sensor point.

The general architecture, outlined in Fig. 3, provides a means for creating a new detection system that enables electrochemical detection based on local redox cycling and 1024 addressable sensor points incorporated into a small area (40 mm^2) for the comprehensive imaging of electrochemical species [6]. Interdigitated array (IDA) electrodes were incorporated onto glass substrates to arrange a single IDA at each sensor point of the device. IDA electrodes have two interdigitated comb-type arrays, each of which consists of planar and parallel metal fingers.9 When the potential of each comb-type electrode is appropriately controlled, a species oxidized at an electrode finger can be reduced back at the neighboring fingers, resulting in redox cycling for amplification of the electrochemical signal. In this study, one comb-type electrodes of the IDA connected to a column electrode and the other to a row electrode.

The device was applied for bioelectrochemical imaging of ALP aggregates. The image followed the position of the ALP aggregate in the solution and the intensity was dependent on the ALP activity of the aggregate (Fig. 4).

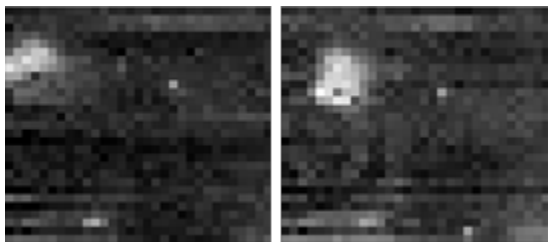

Fig. 4. Electrochemical imaging of ALP. The electrochemical response was acquired after adding the ALP/BSA aggregate (approximately 1-mm diameter) (right image).

Enzymes, such as ALP, were successfully detected using the device; therefore, this device could be used as a comprehensive, high-throughput lab-on-a-chip tool for applications such as enzyme-linked immunosorbent assay (ELISA), reporter gene assay for monitoring gene expressions, DNA analysis, and cell culture array. Although an application of electrochemical potentials to electrodes may be a critical issue for adhesive cells and spheroids, it is unnecessary to bound cells on the electrodes of the device since the device has microwells that can trap cells or spheroids on the sensors for cell assays.

4. Bioimaging with SECM

SECM has been applied for evaluating the enzyme and cellular activity estimating cell membrane permeability and detecting electroactive metabolic chemicals with short life spans. Membrane protein has also been detected with SECM. Miniaturization of the probe electrode is important for improving the temporal and spatial resolution. In addition, a fine distance regulation system is required to approach the probe electrode against live cell surfaces.

Significant efforts have been made to bring the electrode proximate with sample surface. Nevertheless, it was difficult to apply the system to the measurement of soft samples because the force interaction was usually very unstable to serve as a feedback signal. Shear force feedback regulation has also been used for control of the probe electrode sample distance [7]. We reported the simultaneous imaging of the topography and electrochemical signals of single living cells using shear force distance regulation of a ring type nanoelectrode probe. However, preventing probe-cell contact was still difficult because the solution viscosity interfered with the shear force detection. We adopted the feedback regulation used in scanning ion conductance microscopy (SICM) which uses a nanopipette as a scanning probe. SICM is based on the phenomenon that the ion flow through a sharp fluid filled nanopipette is partially occluded when the nanopipette approaches the surface of a sample. Living cell surface topography and dynamic measurements have been performed. Topographical information of the live cell surface can be used to improve the resolution of other analytical tools [8].

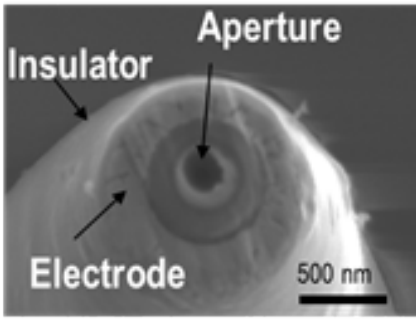

Fig. 5. SEM micrographs of the SECM/SICM probe.

We demonstrate a hybrid syst
and SICM with ion current feedb
of non-contact topography and
nanopipette/nanoring electrode
electrochemical measurement on
pipette had an aperture radius of
ring electrode were 330 and 55
probe was performed with scanr
and approach curve measurement
of topography and electrochemi
(HRP) and glucose oxidase (GC
cardiac myocytes). The measu
enzyme spots on uneven surfa
acquired high resolution topog
electrochemical signals (Fig. 6).
evaluation of the permeability of

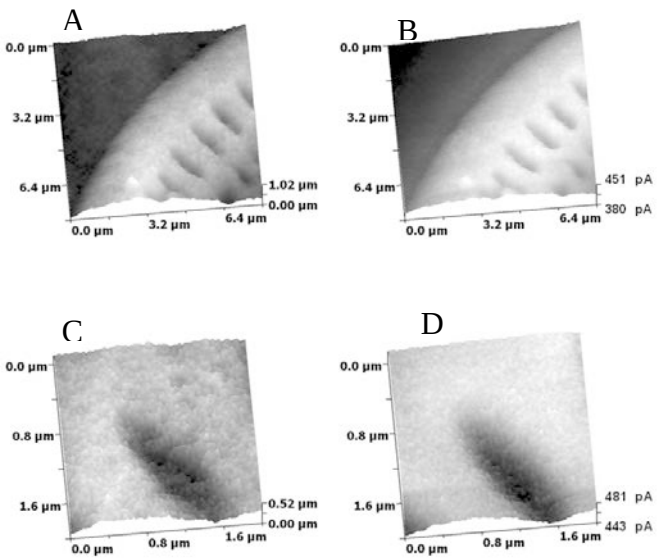

Fig. 6. Topographic (A,C) and electrochemical images (B,D) of a GOD immobilized substrate. Upper and lower images were captured with 8 μm × 8 μm and 2 μm × 2 μm, respectively. The probe-sample distances were held at 100 nm.

Summary

Bioelectrochemical sensing systems with micro/nanoelectrodes has been applied to localized characterization of biomaterials. The results so far obtained clearly indicate that electrochemical measurements afford indispensable information particularly on electron and ion-transfer at various biomolecules-related interfaces. Also, incorporation of modern micro/nanofabrication technologies into electrochemical devices will lead unique bioelectronics devices which ensure the realization of safe and secure society.

References

[1] S. Szunerits, and L. Thouin, "Microelectrode array" in "Handbook of Electrochemistry", Elsevier (2007).

[2] A. J. Bard and M. V. Mirkin, "Scanning Electrochemical Microscopy", Marcel Dekker (2000).

[3] Z. Y. Lin, Y. Takahashi, Y. Kitagawa, T. Umemura, H. Shiku, T. Matsue, Anal. Chem., **80**, 6830 (2008)

[4] Z. Y. Lin,Y. Takahashi, T. Murata, M. Takeda, K. Ino, H. Shiku, T. Matsue, Angew. Chem. Int. Ed., **48**, 2044 (2009)

[5] Z. Y. Lin, K. Ino, H. Shiku, T. Matsue, Chem. Commun., **46**, 559 (2010); Z. Y. Lin, K. Ino, H. Shiku, T. Matsue, G. Chen, Chem. Commun., **46**, 234 (2010).
[6] K. Ino, W. Saito, M. Koide, T. Umemura, H. Shiku, T. Matsue, Lab Chip, in press
[7] Y. Takahashi, T. Miyamotoa, H. Shiku, R. Asano, T. Yasukawa, I. Kumagai, T. Matsue, Anal. Chem., **81**, 2785 (2009); Y. Takahashi, H. Shiku, T. Murata, T. Yasukawa, T. Matsue, Anal. Chem., **81**, 9674 (2009)
[8] Y. Takahashi, Y. Murakami, K. Nagamine, H. Shiku, S. Aoyagi, T. Yasukawa, M. Kanzaki, T. Matsue, Phys. Chem. Chem. Phys., **12**, 1001 (2010)
[9] Y. Takahashi, A. I. Shevchuk, P. Novak, Y. Murakami, H. Shiku, Y. E. Korchev, T. Matsue, J. Am. Chem. Soc., **132**, 10118 (2010)

Nanoporous Metals as Green Catalysts for Molecular Transformations

Naoki Asao

WPI Advanced Institute for Materials Research, Tohoku University

1. Introduction

Molecular metal catalysts (**A**), such as $AuCl(PPh_3)$ and $Pd(PPh_3)_4$, have been used for many molecular transformations as homogeneous catalysts [1]. However, the use of heterogeneous catalysts offers several advantages over homogeneous systems, such as ease of recovery and recycling, atom utility, and enhanced stability. While bulk metals (**D**) are catalytically inert materials, supported nanoscale metal particles (**B**) on suitable oxide show catalytic activities in a variety of molecular transformations [2]. On the other hand, the catalytic properties of unsupported metals, such as nanoporous metal materials (**C**), are still less explored. The nanoporous metal materials can be generally prepared by leaching less noble metals from the corresponding alloys through a route similar to that for the preparation of Raney nickel. For example, nanoporous gold is fabricated from Au-Ag alloy by means of free corrosion in nitric acid [3]. It has an open sponge-like morphology of interconnecting ligaments on the nanometer length scale. Our research focused on these nanoporous metal materials as promising green catalysts.

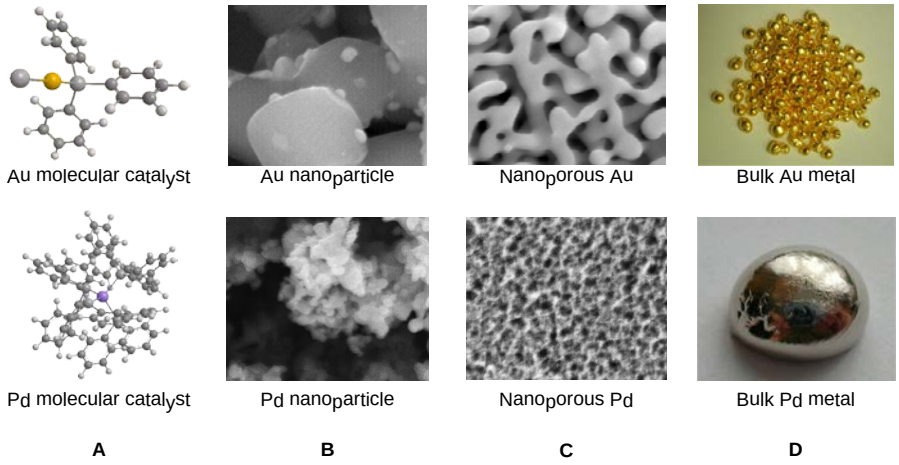

Fig. 1 Four different types of morphology of gold and palladium.

2. Results and discussion

2.1 AuNPore-catalyzed benzannulation

We initially examined the catalytic activity of the nanoporous gold by use of the

[4+2] benzannulation reaction between *ortho*-alkynyl benzaldehyde **1** and phenylacetylene **2** as a model reaction, which has been previously reported by our group with homogeneous gold catalysts [4]. The reaction proceeded with 20 mol % of AuNPore-1, having around 25 nm pore size, at 150 ^{o}C for 2.5 h, and the desired product **3** was obtained in 62 % yield together with a small amount of decarbonylated naphthalene derivative **4** (Scheme 1). On the other hand, any reactions did not take place in the absence of the catalyst or in the presence of the non-dealloyed $Au_{30}Ag_{70}$ thin plates. These results clearly indicated that the nanoporous structure of the catalyst is necessary for this transformation [5].

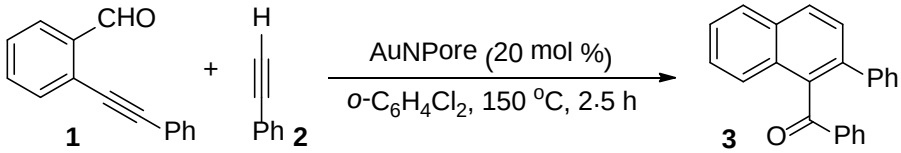

Entry	Average pore size		Yield of **3** (%)
1	AuNPore-1	25 nm	62
2	reuse 1		61
3	reuse 2		60
4	AuNPore -2	30 nm	61
5	AuNPore -3	40 nm	12
6	AuNPore -4	60 nm	trace
7	AuNPore -5	100 nm	0

Scheme 1 AuNPore-catalyzed benzannulation reaction between *ortho*-alkynyl benzaldehyde **1** and phenylacetylene **2**.

AuNPore can be recovered simply by picking up with tweezers because the catalyst is a bulk metal. Therefore, unlike ordinary heterogeneous catalysts, any cumbersome work-up procedures, such as filtration or centrifugation, are not required. The catalyst can be reused several times and the chemical yields of **3** were constantly good in each case (entries 1-3). We found that the catalytic activity of the nanoporous gold was highly dependent on the pore size in this transformation. AuNPore-2, having around 30 nm pore size, exhibited the similar activity with AuNPore-1 (entry 4). However, the chemical yields were dramatically decreased with catalysts having more than 40 nm pore sizes (entries 5-7).

2.2 AuNPore-catalyzed oxidation of organosilanes with water

These results mentioned above prompted us to further explore the feasibility of

carrying out a wide range of molecular transformations with this material. Then, we next examined the oxidation of organosilanes with water, leading to silanols, which are useful building blocks for silicon-based polymeric materials as well as nucleophilic coupling partners in organic synthesis. Although several metal particles have been reported as catalysts for this transformation, there are some drawbacks in those cases, such as poor long-term stability, narrow substrate generality, formation of by-products, and complicated work-up procedure for separation of products from the catalyst [6]. We found that the nanoporous gold exhibited a remarkable catalytic activity in the oxidation of $PhMe_2SiH$ **5** and the corresponding silanol **6** was produced quantitaively under mild conditions together with the evolution of hydrogen gas (Scheme 2) [7]. The formation of by-products, such as disiloxane, was not detected at all by GCMS. The turnover frequency (TOF) of 3.0 s^{-1} was achieved in this catalytic system. The catalyst can be used at least 5 times repeatedly and the product was obtained nearly quantitatively every time (entries 1-5). The turnover number (TON) reached up to 10700. SEM images of the AuNPore catalyst (Fig. 2) indicate that there is no difference on the surface of the catalyst before and after 5 times use.

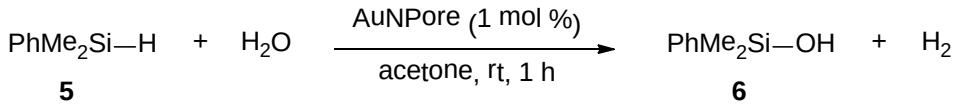

Entry	Catalyst	Yield of **6** (%)
1	fresh	100
2	reuse 1	98
3	reuse 2	100
4	reuse 3	99
5	reuse 4	100

Scheme 2 AuNPore-catalyzed oxidation of $PhMe_2SiH$ with water.

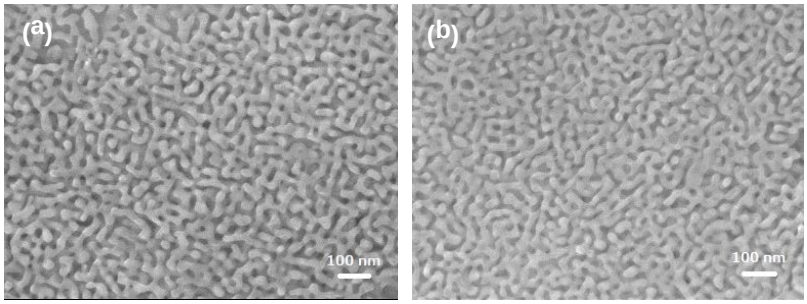

Fig. 2 Scanning electron microscopy (SEM) images of AuNPore: a) before reaction, b) after being used five times for oxidation of $PhMe_2SiH$.

The catalytic oxidation reactions with a variety of organosilanes were conducted and representative examples are shown in Fig. 3. Not only aromatic silanes but also sterically hindered trialkylsilanes were oxidized effectively. The AuNPore catalyst was also applicable to the oxidations of tri-, di-, and mono-phenylsilanes, and the corresponding oxygenated products were obtained in high yields, respectively. Alkenyl- and alkynyl-containing silanes were oxidized smoothly without reduction of their multiple bonds by H_2 gas.

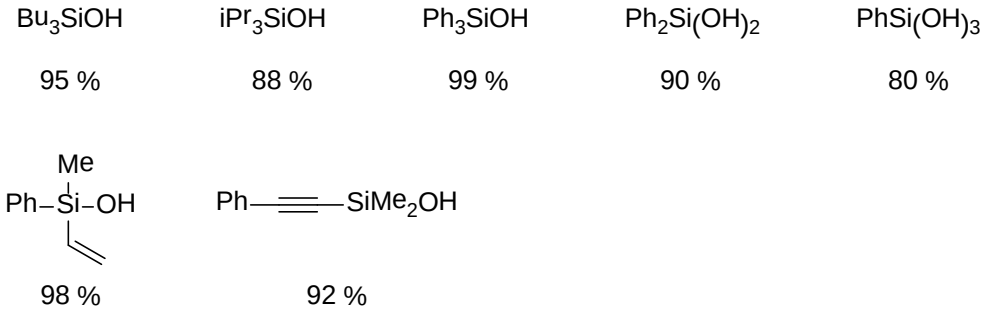

Fig. 3 Representative examples for AuNPore-catalyzed oxidation of organosilanes.

Leaching test was conducted to clarify whether the disolved gold species in solvents take part in the current reaction system or not. After the catalytic oxidation of **5** was carried out for 10 min under the standard condition, AuNPore catalyst was removed from the reaction vessel. ^{1}H NMR analysis of the mixture showed that **6** was produced in 48% yield at this time. While stirring of the mixture was continued in the absence of the catalyst for 50 min, further consumption of **5** was not detected at all. Then, the AuNPore was put back into the mixture. The oxidation reaction started again and finally **6** was obtained in 99% yield with 50 min. Furthermore, leaching of the gold in the reaction of **5** was not detected by inductively coupled plasma (ICP) analysis (<0.0005%). These results clearly indicated that the current transformation was catalyzed by the AuNPore catalyst but not by the dissolved gold species in solvents.

2.3 PdNPore-catalyzed Suzuki coupling

In parallel with the study on AuNPore, the catalytic property of nanoporous palladium (PdNPore) has been investigated. This material can be easily fabricated from metallic glassy ribbons $Pd_{30}Ni_{50}P_{20}$ [8] by electrochemical dealloying process [9]. The resulting PdNPore was used as a catalyst in the Suzuki-coupling reaction, which is one of the most important organic transformations in recent years [10]. The reaction of iodobenzene **7** with *p*-tolylboronic acid **8** using KOH as a base in the presence of 2 mol% PdNPore gave the corresponding biphenyl product **9** in a nearly quantitative yield

(Scheme 3, Entry 1). On the other hand, no coupling products were obtained in the presence of un-dealloyed (non-porous) metallic glass $Pd_{30}Ni_{50}P_{20}$ or in the absence of PdNPore [11].

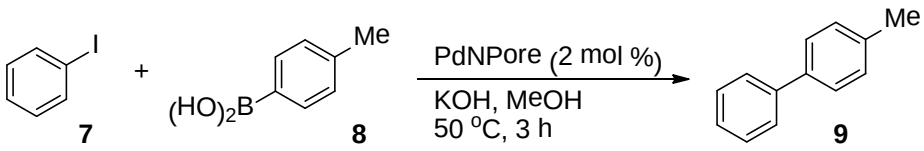

Entry	Catalyst	Yield of **9** (%)
1	fresh	99
2	reuse 1	94
3	reuse 2	92
4	reuse 3	95

Scheme 3 PdNPore-catalyzed Suzuki-coupling reaction.

Recently, small palladium particles, consisting of gathering of palladium atoms, have been used as a solid state catalyst. However, a drawback of this catalyst is that it undergoes quite easy agglomeration under the reaction conditions, leading to deactivation of the catalyst. Hence, appropriate stabilizer or supporter is necessary to prevent deactivation by agglomeration. In contrast, PdNPore exhibited an excellent catalytic activity under mild reaction conditions without any supporter, ligand, or stabilizer. Although palladium black has been reported as an unsupported catalyst for Suzuki coupling reaction, nearly one-half equivalent of catalyst is necessary probably due to the poor catalytic activity. Recovery of ordinary heterogeneous catalysts often requires complicated treatment. In contrast, the recovery process in the current catalytic system is simple. Since the size of the catalyst is relatively large, the catalyst and the product can be separated easily by just removal of the liquid moiety by a pipette. The recovered catalyst was washed with MeOH several times and it was reused without further purification. Indeed, the product **9** could be obtained in excellent yield every time when the reactions were performed 4 times repeatedly. Furthermore, SEM images of the catalyst before and after 4 times run indicated the nanoporous structure was maintained well (Fig. 4).

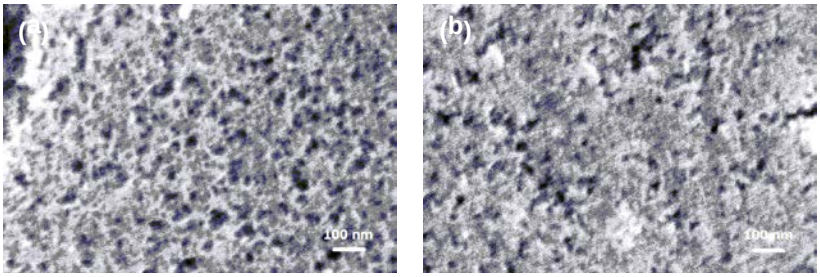

Fig. 4 Scanning electron microscopy (SEM) images of PdNPore: a) before reaction, b) after being used four times for Suzuki coupling between **7** and **8**.

Since leaching of toxic palladium causes contamination of the final products with the dissolved palladium, catalytic systems with low leaching are highly desirable. Inductivity coupled plasma (ICP-AES) analysis did not detect the leaching of the palladium (< 0.0005%) during or after reaction of **7** with **8**. We next checked the leaching by conducting the reaction with the supernatant as follows: The reaction of **7** with **8** was carried out for 30 min under the standard condition, then a half amount of solution was picked up. ^{1}H NMR analysis of the supernatant indicated that **9** was produced in 3% yield at this time. The supernatant was stirred in the absence of the catalyst for 3 h; the chemical yield of **9** at this moment was 24%. On the other hand, stirring of the residual reaction mixture having the catalyst for 3 h gave **9** in 93% yield. These results clearly indicated that dissolved Pd species existed and catalyzed the reaction but its activity was much lower than that of solid state of the catalyst due to the low leaching amount.

The Suzuki-coupling reactions using various aryliodides and arylboronic acids were examined and representative examples are shown in Fig. 5. The reaction proceeded smoothly even with sterically hindered 2-iodoanisole. The reactions of aryl iodides possessing electron-withdrawing groups proceeded faster than those having electron-donating groups. In contrast, the reactions of arylboronic acids possessing electron-donating groups proceeded faster than those having electron-withdrawing groups. Not only aryl iodides but also aryl bromides are suitable substrates.

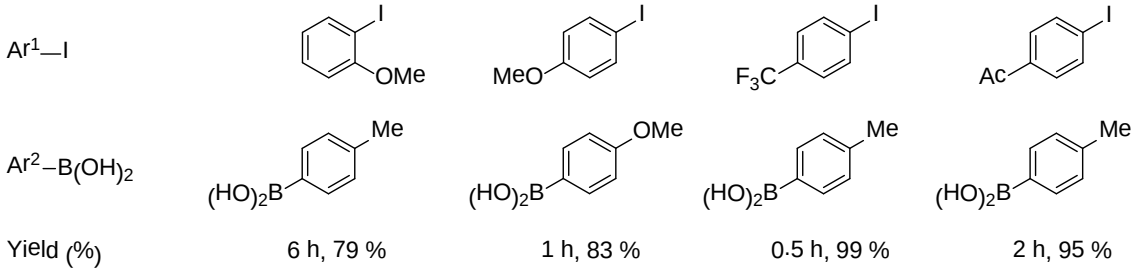

Fig. 5 Representative examples for PdNPore-catalyzed Suzuki coupling.

2.4 PdNPore-catalyzed Heck reaction

The material was next applied to Heck reaction, which is widely utilized in organic synthesis from small scale to the industrial process (Scheme 4) [12]. The reaction of iodobenzene **7** with acrylic acid **10** using KOH as a base in the presence of 2 mol % of PdNPore gave cinnamic acid **11** in 84 % yield (Entry 1). Addition of tetra-*n*-butylammonium iodide (TBAI) improved the chemical yield up to 94% (Entry 2). Since TBAI is known as a stabilizer of Pd particles, it might stabilize the dissolved Pd species

even in the case of the current catalytic system. On the other hand, no coupling products were obtained at all in the absence of PdNPore catalyst or in the presence of un-dealloyed metallic glass $Pd_{30}Ni_{50}P_{20}$ ribbon [13].

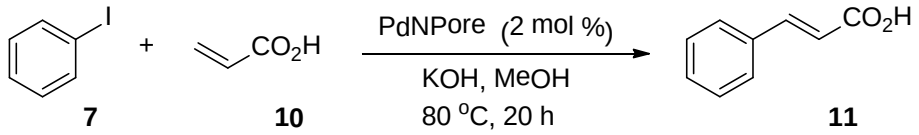

7 **10** **11**

Entry	Additive	Yield of **11** (%)
1	-	84
2	TBAI	94

Scheme 4 PdNPore-catalyzed Heck reaction.

Not only aryliodides, but also less reactive arylbromides were suitable substrates by using Köhler's condition (Scheme 5) [14]. Treatment of 4-bromoacetophenone **12** with styrene **13** in the presence of 2 mol % of PdNPore in *N*,*N*-dimethylacetamide (DMAc) resulted in the formation of **14** in a nearly quantitative yield (Entry 1). Heck reaction is well known to be catalyzed by Pd/C, which is one of the most accessible heterogeneous Pd catalysts. However, it has a serious limitation on the recyclability [14]. In contrast, our catalyst can be used at least 5 times. SEM analysis of the catalyst clearly indicated that nanoporous structures were maintained well even after 5 runs. Furthermore, any significant changes of the composition of the catalysts were not observed before and after reaction by energy-dispersive X-ray (EDX) analysis. These results clearly indicate that PdNPore is a robust and recyclable catalyst for Heck reaction.

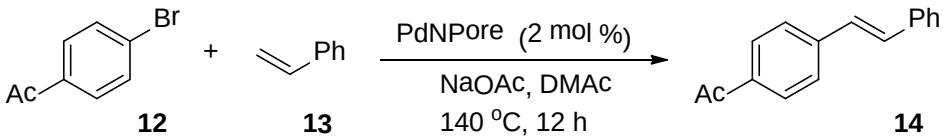

12 **13** **14**

Entry	PdNPore	Yield of **14** (%)
1	Fresh	99
2	Reuse 1	99
3	Reuse 2	99
4	Reuse 3	99
5	Reuse 4	99

Scheme 5 PdNPore-catalyzed Heck reaction of bromoarene.

The representative examples are shown in Fig. 6. While the reactions of aryliodides were not influenced significantly by the electronic effect of the substituents on the aryliodides, the reaction speed of arylbromides was considerably dependent on the

substituents on bromoarenes.

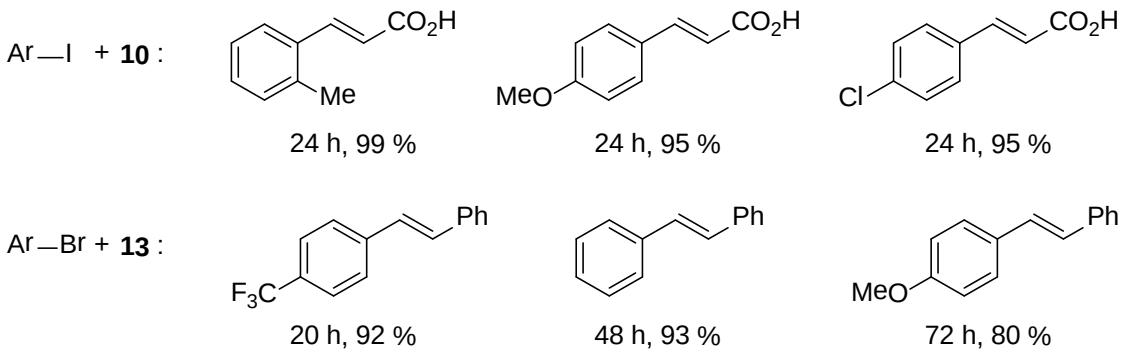

Fig. 6 Representative examples for PdNPore-catalyzed Heck reaction.

We compared the leaching amount of Pd from PdNPore, Pd/C, and Pd black catalysts in the reaction of **12** and **13** by inductivity coupled plasma mass spectrometry (ICP-MS). On the basis of the average of specific surface areas of these catalysts, the leaching amounts of Pd per unit surface area can be calculated and the results are summarized in Table 1. Obviously, the leaching amount from the PdNPore catalyst is significantly smaller than those from the other two commercially available catalysts. This result clearly indicated that PdNPore has higher resistant property against leaching than the other two catalysts. Köhler reported that the Pd concentration in solution in the Pd/C-catalyzed reaction was highest at the beginning of the reaction and was a minimum at the end of the reaction by the reprecipitation of Pd onto the support [14]. It is worth mentioning that the leaching amount from the unsupported PdNPore is smaller than that from the supported Pd/C even at the end of the reaction.

Table 1 Leaching amount of Pd at the end of the reaction with **12** and **13** by use of Pd NPore, Pd black, and Pd/C catalysts.

Pd cat	Leaching amount in solution [μg]	Average of specific surface area [m^2/g]	Leaching amount per unit surface area [μg/m^2]
PdNPore	0.57	13	43.8
Pd black	3.80	50	76.0
Pd/C (10 wt%)	48.2	83	580.7

3. Summary

We have demonstrated that nanoporous gold and palladium are promising nanostructured skeleton catalysts for molecular transformations. Any supports, ligands, or stabilizers are not required in these catalytic systems. The catalysts can be easily

recovered by simple separation processes and the recovered catalysts were reusable without significant loss of catalytic activities. The exploration of new catalytic properties of a variety of nanoporous metals as well as designing and creation of novel types of nano-structured skeleton catalysts are in progress.

Acknowledgements

The author is grateful to Y. Yamamoto, S. Tanaka, M. Chen, W. Zhang, and A. Inoue for their collaboration in this work.

References

1. (a) A. S. K. Hashmi. *Chem. Rev.* **107**, 3180 (2007); (b) N. T. Patil, Y. Yamamoto. *Chem. Rev.* **108**, 3395 (2008); (c) Y. Yamamoto. *J. Org. Chem.* **72**, 7818 (2007); (d) A. S. K. Hashmi. *Angew. Chem. Int. Ed.* **49**, 5232 (2010); (e) L. Yin, J. Liebscher. *Chem. Rev.* **107**, 133 (2007); (f) Y. Tsuji, T. Fujihara. *Inorg. Chem.* **46**, 1895 (2007).
2. (a) C. Della Pina, E. Falletta, L. Prati, M. Rossi. *Chem. Soc. Rev.* **37**, 2077 (2008); (b) A. Corma, H. Garcia. *Chem. Soc. Rev.* **37**, 2096 (2008); (c) M. Seki. *Synthesis* 2975 (2006).
3. (a) A. J. Forty. *Nature* **282**, 597 (1979); (b) J. Erlebacher, M. Aziz, A. Karma. *Nature* **410**, 450 (2001).
4. (a) N. Asao, K. Takahashi, S. Lee, T. Kasahara, Y. Yamamoto. *J. Am. Chem. Soc.* **124**, 12650 (2002); (b) N. Asao, T. Nogami, S. Lee, Y. Yamamoto. *J. Am. Chem. Soc.* **125**, 10921 (2003); (c) N. Asao. *Synlett*, 1645 (2006).
5. N. Asao, Menggenbateer, Y. Seya, Y. Yamamoto, M. Chen, W. Zhang, A. Inoue. *Synlett* in press (DOI: 10.1055/s-0031-1289527).
6. (a) K. Mori, M. Tano, T. Mizugaki, K. Ebitani, K. Kaneda. *New J. Chem.* **26**, 1536 (2002); (b) E. Choi, C. Lee, Y. Na, S. Chang. *Org. Lett.* **4**, 2369 (2002); (c) T. Mitsudome, S. Arita, H. Mori, T. Mizugaki, K. Jitsukawa, K. Kaneda. *Angew. Chem. Int. Ed.* **47**, 7938 (2008); (d) B. P. S. Chauhan, A. Sarkar, M. Chauhan, A. Roka. *Appl. Organomet. Chem.* **23**, 385 (2009); (e) T. Mitsudome, A. Noujima, T. Mizugaki, K. Jitsukawa, K. Kaneda. *Chem. Commun.* 5302 (2009).
7. N. Asao, Y. Ishikawa, N. Hatakeyama, Menggenbateer, Y. Yamamoto, M. Chen, W. Zhang, A. Inoue. *Angew. Chem. Int. Ed.* **49**, 10093 (2010).
8. J. Yu, Y. Ding, C. Xu, A. Inoue, T. Sakurai, M. Chen. *Chem. Mater.* **20**, 4548 (2008).

9. Y. Zeng, N. Nishiyama, T. Wada, D. Louzguine-Luzgin, A. Inoue. *Mater. Trans.* **47**, 175 (2006).
10. For reviews, see: (a) N. Miyaura, A. Suzuki. *Chem. Rev.* **95**, 2457 (1995); (b) A. Suzuki. *J. Organomet. Chem.* **576**, 147 (1999); (c) S. Kotha, K. Lahiri, D. Kashinath. *Tetrahedron* **58**, 9633 (2002); (d) F. Bellina, A. Carpita, R. Rossi. *Synthesis* 2419 (2004); (e) A. Suzuki. In *Modern Arene Chemistry* (D. Astruc, ed.), p. 53. Wiley-VCH, Weinheim (2002).
11. S. Tanaka, T. Kaneko, N. Asao, Y. Yamamoto, M. Chen, W. Zhang, A. Inoue. *Chem. Commun.* **47**, 5985 (2011).
12. For reviews, see; (a) N. J. Whitcombe, K. K. Hii, S. E. Gibson. *Tetrahedron* **57**, 7449 (2001); (b) A. B. Dounay, L. E. Overman. Chem. Rev. **103**, 2945 (2003); (c) F. Alonso, I. P. Beletskaya, M. Yus. *Tetrahedron* **61**, 11771 (2005).
13. T. Kaneko, S. Tanaka, N. Asao, Y. Yamamoto, M. Chen, W. Zhang, A. Inoue. *Adv. Synth. Catal.* **253**, 2927 (2011).
14. (a) K. Köhler, R. G. Heidenreich, J. G. E. Krauter, J. Pietsch. *Chem. Eur. J.* **8**, 622 (2002); (b) R. G. Heidenreich, J. G. E. Krauter, J. Pietsch, K. Köhler. *J. Mol. Catal. A Chem.* **182-183**, 499 (2002).

Exploring new spintronics materials via investigation of fast precessional spin dynamics using an ultrashort pulse laser

Shigemi Mizukami and Terunobu Miyazaki
WPI Advanced Institute for Materials Research, Tohoku University

1. Introduction

Since the discovery of giant magnetoresistance (GMR) by P. Grünberg and A. Fert [1,2] who obtained the Nobel prize in 2007, spintronics research field increased year by year. One big breakthrough is a finding of large tunnel magnetoresistance (TMR) at room temperature in magnetic tunnel junctions (MTJs) in 1995 [3,4]. The MTJs consist of a few nano meter thick insulating barrier sandwiched by ferromagnetic layers and exhibit, basically, a larger (smaller) resistance in parallel (anti-parallel) configuration of magnetizations. This implies that a MTJ can be used for a non-volatile magnetic random access memory (MRAM) element if a high or low resistance states is regarded as “1” or “0” digital memory bit.

Another interesting proposal was brought in 1996 into spintoronics is the so-called spin-transfer-torque (STT) effect [5]. Conducting electrons flowing through a fixed magnetic layer in a magnetoresistive device are spin polarized along the magnetization. When these spin-polarized electrons pass through another magnetic layer, the polarization direction may have to change depending on relative orientation. In this process, the magnetic layer experiences a torque associated with the transfer of spin angular momentum from conducting electrons. For large current, the spin torque amplifies the cone angle of spin precession and leads magnetization switching in the case that the spin torque overcomes magnetic damping. Thus, the magnetization of nano-scaled free layer is controllable by the flowing current direction.

Nowadays, the researchers in spintronics field are developing STT-MRAM utilizing the above two fundamental technologies. The features of STT-MRAM is not only non-volatility but also a large memory capacity and a high speed in reading and storing of digital memory, comparable to a dynamic random access memory (DRAM) and/or static RAM (SRAM), made of CMOS technology [6]. STT-MRAM is considered to be an important element of Normally-off computer as Green Technologies in near future. However, there are many subjects to be overcome for realization of such an ultimate memory. One of the important subjects is to develop the new magnetic materials with low magnetic damping as well as high perpendicular magnetic anisotropy, and also to clarify their mechanism.

2. Perpendicular magnetic anisotropy and magnetic damping

When the magnetic materials are patterned into several tens nano meter scale, that is comparable to the current CMOS technology node, magnetization direction fluctuates randomly against time, like as the Brownian motion of very small particle. Reducing of these thermal fluctuations of magnetization is crucial to make nano scaled memory because the thermal fluctuation of magnetization leads to lose a stored digital memory in MRAM. To avoid it, a magnetic material with a large perpendicular magnetic anisotropy is used in electrodes of MTJ. Thermal fluctuation of magnetization is stabilized significantly by high perpendicular magnetic anisotropy [7]. There have been several magnetic materials with high perpendicular magnetic anisotropy, so far, because such materials are also used in a storage media in hard disk drive or permanent magnet. Most of such magnetic materials have crystal structures with symmetry lower than a cubic, i.e., tetragonal or hexagonal. Artificial magnetic multilayer also shows perpendicular magnetic anisotropy owing to two dimensional structures [7]. Most of them contain various rare earth or noble metals. History of research on magnetic anisotropy is long [8] and the development of precise *ab-initio* calculation and progress of microscopic characterization based on X-ray reveals the mechanism of anisotropy in last two decade, but physics of magnetic anisotropy was not so clear yet.

In the elementary mechanics, we learn that a friction forces to stop an object moving in the air and this friction force is proportional to velocity of moving object. Such friction is a universal phenomenon that appears from microscopic to macroscopic scale. Large friction needs large power to drive the motion of object, but a finite friction is necessary to control it, thus friction control is very important technology to save the energy, as seen in a hybrid car. Similarly, magnetization also feels a friction inside magnets, so-called magnetic damping. In STT-MRAM, small magnetic friction is efficient to drive the magnetization motion with saving the power requiring magnetization reversal [6]. Origin of magnetic friction can be attributed to one electron spin relaxation phenomena related quantum-mechanical spin-orbit interaction [9], but there are a few data of magnetic damping in the magnetic materials with perpendicular magnetic anisotropy and the related physics is not yet understood fully.

Theories show magnetic friction and magnetic anisotropy originates from spin-orbit interaction, namely materials with large magnetic anisotropy might tend to show large magnetic friction. Therefore, it is a challenging task to explore new materials suitable to STT-MRAM.

3. Spin dynamics and all-optical time-resolved magneto-optical Kerr effect

The objectives of our studies are to get insight into physics of magnetic damping in magnetic materials with large perpendicular magnetic anisotropy and also to explore magnetic materials with both high perpendicular magnetic anisotropy and small magnetic damping. However, it is difficult to evaluate magnetic damping constant in such magnetic materials. A basic motion of spin in magnets is precession, which is similar to oscillation of a pendulum. Precession frequency is roughly proportional to the perpendicular magnetic anisotropy field. Precession frequency is several GHz for the usual ferromagnetic metals, e.g., iron, but it exceeds more than 100 GHz in the magnetic materials with high perpendicular magnetic anisotropy. "All optical pump-probe detection" is the current state of art technique for the investigation of spin dynamics [10]. All optical pump-probe detection is based on pump-probe technique with femto second laser. The motion of spins can be induced only by laser light pulse and any coils or inductances, which are required to generate pulsed magnetic field in the other techniques, are not involved in the set-up, so that one can achieve the ultimate time resolution better than hundred femto second. The equivalent frequency bandwidth of this measurement is more than 1 THz.

In 2008-2009, we have constructed the set-up of all-optical time-resolved magneto-optical Kerr effect (TRMOKE) using a standard optical pump-probe set-up with Ti: Sapphire laser and regenerative amplifier (wavelength of 800 nm, pulse width less than 100 fs) [11,12]. S-polarized probe light is normally incident on a film surface. A very small amount of rotation of polarization vector of laser light reflected from sample is

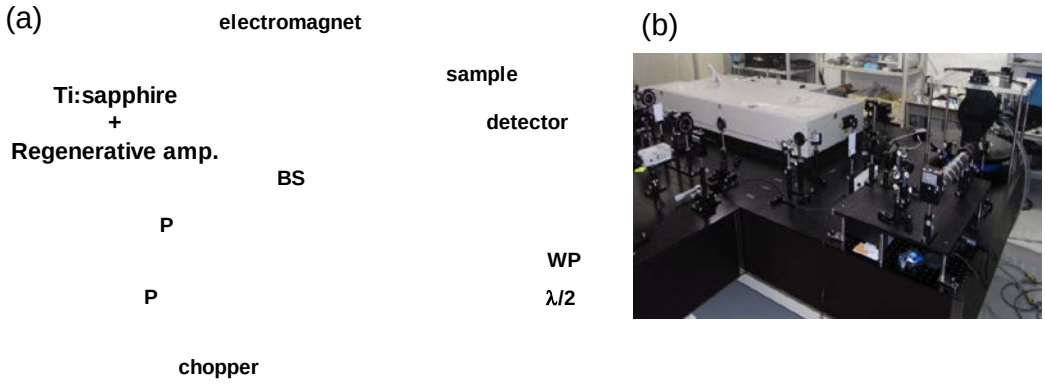

Figure 1. (a) Schematic illustration of optical set-up. P, WP, and BS correspond to a polarizer, beam splitter, and Wollaston prism as an analyzer. Thin and bold red lines are probe and pump beam path, respectively. (b) the photograph of optical set-up constructed in Integration laboratory in WPI-AIMR.

detected by a balanced detector after passing though analyzer (Wollaston prism) by polar magneto-optical Kerr effect (PMOKE). Intense pump beam is also focused to the sample overlapped and delayed by probe beam and time variation of magnetization was detected. Magnetic field can be applied up to 10 kOe and the field direction can be varied from in-plane to out-of-plane. Hereafter, we discuss the result of investigation of fast spin precession dynamics in various magnetic films with large perpendicular magnetic anisotropy.

5. Precessional spin dynamics in ultrathin films and multilayers exhibiting a large perpendicular magnetic anisotropy

As mentioned earlier, artificial layered materials have a large uniaxial magnetic anisotropy induced by symmetry broken at an interface. We investigated Co-based multilayered structure: Co/Pd [13] and Co/Ni [14], here we show representative results of very thin Co layer sandwiched by Pt layer [15].

Films were deposited on a naturally oxidized Si substrate using an ultra-high vacuum magnetron sputtering system at room temperature. Thickness of buffer and capping layer of Pt were 5 and 2 nm, respectively, and Co layer thickness was varied from 4 to

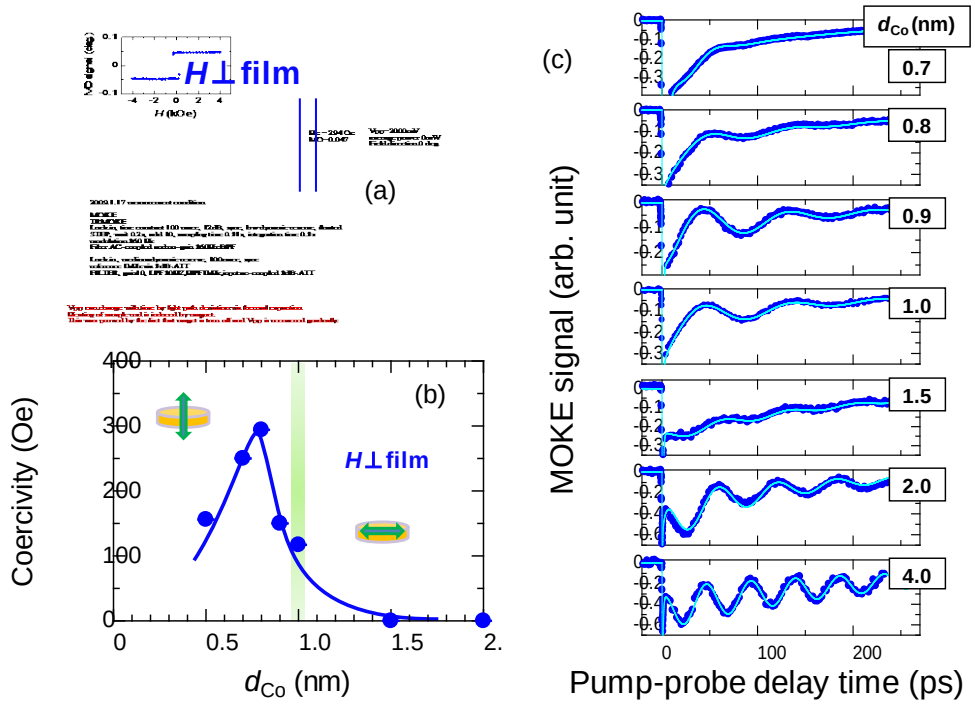

Figure 2 (a) Typical hysteresis curves for a Pt/Co/Pt trilayer film with Co layer thickness d_{Co} of 0.8 nm. (b) Co layer thickness dependence of Coercivity, and (c) time-resolved magneto-optical Kerr effect signal for the films with different d_{Co}.

0.5 nm. A typical hysteresis loop for a film with Co layer thickness of 0.8 nm is shown in Fig. 2(a), in which a coercivity H_C was ~ 300 Oe and an effective perpendicular magnetic anisotropy field H_k^{eff} was 2.1 kOe. Figure 2(b) shows the coercivity as a function of Co layer thickness evaluated from PMOKE measurements, confirming that Pt/Co/Pt films was magnetized perpendicularly at Co layer thickness $d_{Co} < 1$ nm. Time-resolved magneto-optical signals for these films are shown in Fig. 2(c). Signal shows a rapid decrease in sub-ps time regime and then exhibits damped oscillation, those correspond to ultrafast demagnetization due to pulse heating and magnetization precession, respectively. Spin precession signals are observed clearly in all films, especially in case of perpendicularly magnetized films where cobalt layer thickness is comparable to a few atomic layers. Precession signal decays more rapidly in a film with thinner Co layer thickness, which implies magnetic friction acts more strongly on spins in a few atomic layers of cobalt. To determine magnetic damping quantitatively, the precession frequency f and decay time τ for Pt/Co/Pt films were evaluated from the time-resolved data by fitting the damped harmonic function, and then the experimental data of f and $1/\tau$ were analyzed by using Landau-Lifshitz-Gilbert equation, a basic equation of motion of magnetization:

$$\frac{d\boldsymbol{m}}{dt} = -\gamma \boldsymbol{m} \times \boldsymbol{H}_{eff} + \alpha \boldsymbol{m} \times \frac{d\boldsymbol{m}}{dt}. \qquad (1)$$

Here, $\boldsymbol{m}$, γ, $\boldsymbol{H}_{eff}$, and α are the unit vector of magnetization direction, the gyromagnetic ratio, the effective magnetic field, and the dimensionless damping constant. Extracted damping constant α increases, up to 0.4, with decreasing Co layer thickness, those values are by a factor of 10-100 larger than those in the ordinary magnetic materials, such as iron. This means that huge electric power needs to control magnetization direction of Co layer in these films.

6. Ultrafast precessional spin dynamics in Mn-Ga alloys

As mentioned earlier, some types of magnetic materials naturally forms atomically layered structure that leads to tetragonal distortion of crystal lattice, or some types of magnetic materials have hexagonal lattice. These crystal structures have an axial symmetry, leading a uniaxial magnetic anisotropy along c-axis. In case that those films are textured along c-axis, perpendicular magnetic anisotropy appears. A hexagonal CoCrPt and tetragonal FePt alloys are, respectively, the materials used in the storage media currently and possibly near future, so that we investigated magnetization

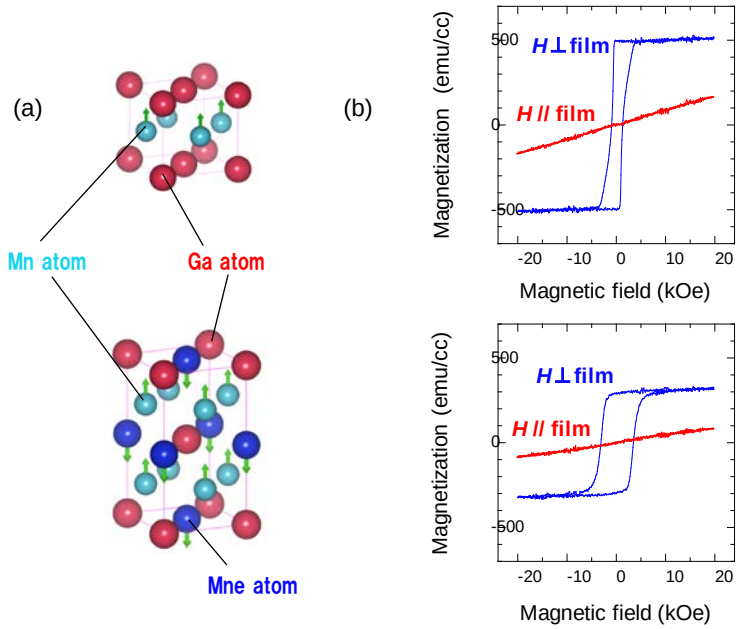

Figure 4. (a) Schematic illustration of crystal structure of $L1_0$-MnGa and $D0_{22}$-Mn_3Ga. (b) Typical hysteresis curves for the films having $L1_0$ or $D0_{22}$ crystal structures.

dynamics in those materials [16-18]. Here, we show only the recent result of Mn-Ga alloy films [19].

A Mn-Ga binary alloy has a tetragonal crystal structure and large uniaxial anisotropy [Fig. 1(a)], that is similar to that for a FePt alloy. This material contains no noble and rare-earth metals which are important constituents to gain high magnetic anisotropy, such as FePt or $Nd_2Fe_{14}B$. Curie temperature for Mn-Ga alloys is much higher than room temperature, and the large spin polarization has also been predicted in Mn_3Ga [20], nevertheless those contain no magnetic elements, i.e., Fe, Co, and Ni. We succeeded, for the first time, to grow $Mn_{2.5}Ga$ epitaxial film using ultra-high vacuum magnetron sputtering technique and reported a huge uniaxial perpendicular magnetic anisotropy constant over 10 Merg/cc with low saturation magnetization ~ 250 emu/cm^3 [21]. High-TMR ratio has also been predicted by our group [22]. However, there are many open questions, especially magnetic damping constant.

Figure 4(b) shows the typical hysteresis loops for the Mn-Ga films with different composition with applying field of out-of-plane (in-plane) denoted by red (blue) curves. Both films show good perpendicular uniaxial anisotropy and very large effective anisotropy field H_k^{eff}, close to 10 T, was estimated from the hysteresis loops. Figure 5(a) shows the typical time-resolved magneto-optical Kerr signals for the films. Sinusoidal oscillations correspond to magnetization (spins) precessions about an

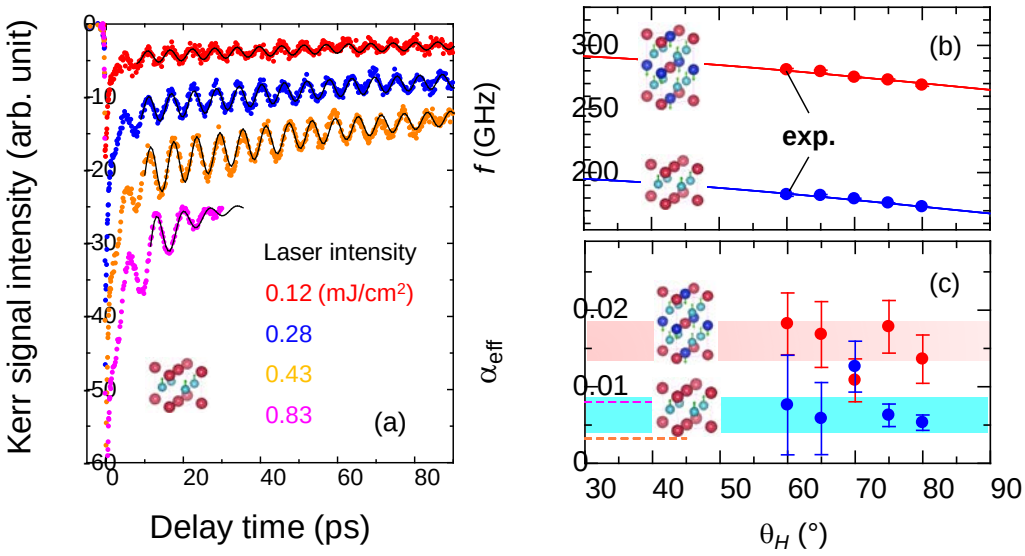

Figure 5 (a) Typical example of time-resolved magneto-optical Kerr effect of the Mn-Ga film with $L1_0$ structure. Magnetic field direction θ_H dependence of (b) precession frequency and (c) effective damping constant for $L1_0$ and $D0_{22}$ Mn-Ga films.

externally applied magnetic field. Spin precessions show ultrafast frequencies over 100 GHz with no remarkable decays, that have never been observed in metallic ferromagnets, so far.

Precession frequency f are extracted from the data are shown in Fig. 5(b) as a function of magnetic field direction. Experimental data of f are well fitted to the data calculated from eq. (1) with adequate fitting parameters. The damping constants α are also extracted from the data [Fig. 5(c)], average values of 0.015 and 0.0075, respectively, for $L1_0$ and and $D0_{22}$ Mn-Ga alloys. First-principles calculations are also in qualitative agreement with these experimental results [19].

4. Discussion

The damping constants for various films with perpendicular magnwetic anisotropy are plloted as a function of the perpendicular anisotropy constant in Fig. 6. The reported materials with large perpendicular magnetic anisotropy show large damping constants as shown in Fig. 6. However, damping constants for Mn-Ga alloys are by a factor of ten smaller than known materials even though this materials have a large perpendicular magnetic anisotropy. As we mentioned earlier, the origin of both perpendicular magnetic anisotropy and magnetic damping relate to quantum mechanical spin-orbit interaction from the theoretical points of view [8,9]. Thus, the compatibility of small damping and large perpendicular magnetic anisotopry in Mn-Ga alloys is not only

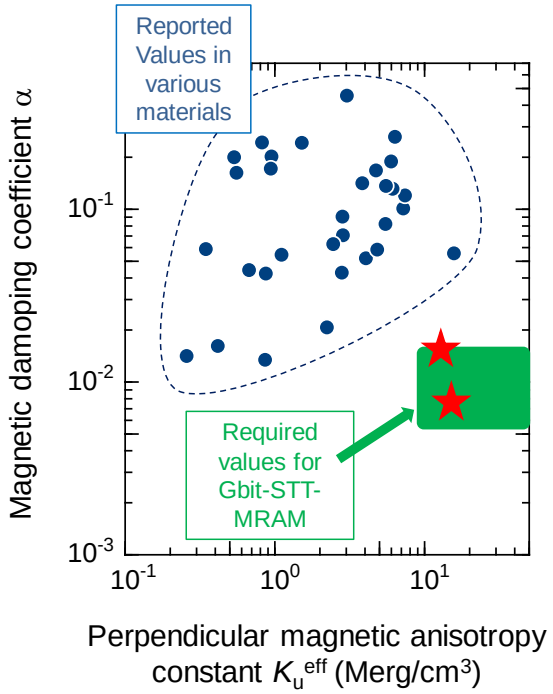

Figure 6 Magnetic damping constant α as a function of effective uniaxial perpendicular magnetic anisotropy constant K_u^{eff} for various types of perpendicular magnetization films.

technologically but also fundamentally interesting. One reason of small damping is that this alloy has small density of states at Fermi level and no constituent of heavy elements [19,23]. Full understanding needs further investigations.

4. Summary and prospect

We have achieved the construction of set-up, the investigation of dynamics for various magnetic films with perpendicular magnetic anisotropy, and the discovery of excellent properties in Mn-Ga alloys. This finding contributes not only to develop STT-MRAM but also to form the new concept for designing *Green Spintronics Materials* with no heavy elements. The Mn-Ga alloys has potentially high spin polarization and exhibit high-TMR ratio, so that it is important to investigate spin transport properties of MTJ with Mn-Ga, such studies are in progress [24].

It is important to continue to explore materials with much better properties for STT-MRAM. Such new materials could be created by controlling atomic layer structure including light element as well as electronic structure around Fermi energy.

It is naturally considered that a high speed motion of spins, demonstrated in our optical experiments in the Mn-Ga films, can be applied to a high speed spintronics device. Such a new devices should be useful for nonvolatile logic application, that is

one of the future directions of research.

Acknowledgements

We sincerely thank our colleagues; F. Wu, E. P. Sajitha, D. Watanabe, T. Kubota, X. Zhang, Q. Ma, M. Araidai, and Prof. M. Tsukada (WPI-AIMR), H. Naganuma, M. Oogane, and Prof. Y. Ando, and Prof. A. Sakuma (Department of Applied Physics), Y. Miura and M. Shirai (RIEC), and J. Walowski (Goettingen University). These studies were partially supported by NEDO Spintronics Nonvolatile Devices Project, Grant-in-Aid for Scientific Research from JSPS and MEXT, Grant for Industrial Technology Research from NEDO, FIRST Program from JSPS, Strategic International Cooperative Program “ASPIMATT” from JST, and Asahi glass foundation.

References

[1] G. Binasch et al. Phys. Rev. B **39,** 4828 (1989).
[2] M. N. Baibich et al., Phys. Rev. Lett., **61,** 2472 (1988).
[3] T. Miyazaki and N. Tezuka, J. Magn. Magn. Matter. **139,** L231 (1995).
[4] J. S. Moodera et al., Phys. Rev. Lett. **74**, 3273 (1995).
[5] J. C. Slonczewski: J. Magn. Magn. Mater. **159,** L1 (1996).
[6] H. Yoda et al., Curr. Appl. Phys. **10,** e87 (2010).
[7] D. Weller et al., IEEE Trans. Magn. **36,** 10 (2000).
[8] P. Bruno, Physical origins and theoretical models of magnetic anisotropy (Ferienkurse des Forschungszentrums Jurich, Jurich, 1993).
[9] V. Kambersky, Can. J. Phys. **48,** 2906 (1970).
[10] M. van Kampen et al. Phys. Rev. Lett. **88,** 227201 (2002).
[11] S. Mizukami et al., Appl. Phys. Express **1,** 121301 (2008).
[12] S. Mizukami et al., J. Conf. Series **200**, 042017-1-4 (2010).
[13] E. P. Sajitha et al., IEEE Trans. Magn. **46,** 2056 (2010).
[14] S. Mizukami et al., Appl. Phys. Express **4,** 013005 (2011).
[15] S. Mizukami et al., Appl. Phys. Lett. **96,** 152502 (2010).
[16] S. Mizukami et al., Appl. Phys. Express **3,** 123001 (2010).
[17] S. Mizukami et al., Appl. Phys. Lett. **98,** 052501 (2011).
[18] S. Mizukami et al., IEEE Trans. Magn. **47**, 3897 (2011).
[19] S. Mizukami et al., Phys. Rev. Lett. 106, 117201 (2011).
[20] B. Balke et al., Appl. Phys. Lett. **90,** 152504 (2007).
[21] F. Wu et al., Appl. Phys. Lett. **94,** 122503 (2009).
[22] T. Kubota et al., Appl. Phys. Express **4,** 043002 (2011).

[23] S. Mizukami et al., Jpn. J. Appl. Phys. **50**, 103003 (2011).
[24] T. Kubota et al., Appl. Phys. Lett. **99**, 192509 (2011).

GI3 VISITING PROFESSOR LIST

Name	Affiliation	Position	Host PI	Term
Daniel Miracle	AF Research Laboratory	Senior Scientist	Louzguine	2011/8/14 - 2011/9/24
Richard Tilley	Victoria University of Wellington	Associate Professor	Ajiri	2012/3/16 - 2012/4/16
Zhang Di	Shanghai Jiao Tong University	Professor	Chen	2012/2/3 - 2012/3/2

GI3 VISITING SCIENTIST LIST

Name	Affiliation	Home PI	Host PI	Term
Jorg Fromel	Fraunhofer Institute ENAS	Gessner	Esashi	2011/5/11 - 2011/11/30
Weichin Lin	University of Cambridge	Gessner	Esashi	2011/12/15 - 2012/3/31
Yu Lang Chu	Chemnitz University of Technology	Gessner	Esashi	2012/2/15 - 2012/9/30
Jia Chenping	Fraunhofer Institute ENAS	Gessner	Esashi	2012/3/8 - 2012/6/29
Yaofeng Guo	Institut Polytechnique de Grenoble	Yavari	Louzguine	2012/2/15 - 2012/4/15
Olga Ivanova	Institut Polytechnique de Grenoble	Yavari	Louzguine	2012/2/15 - 2012/4/15